Power uprates
and plant life extension

CASL-U-2011-0186-000

Consortium for Advanced Simulation of LWRs

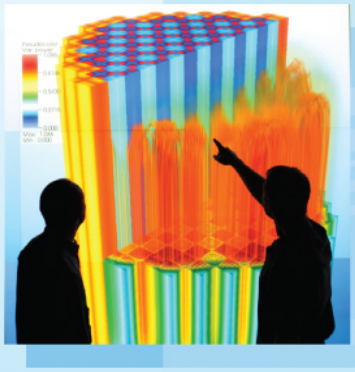

Engineering design
and analysis

Implementation of the Transient Capability in MPACT: Phase II

Science-enabling
high performance
computing

Yunlin Xu, Ang Zhu, Aaron Graham, Andrew Gerlach, Liangzhi Cao, Tom Downar, John Lee

University of Michigan

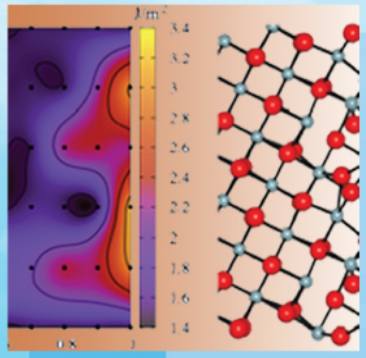

Fundamental science

September 30, 2014

Plant operational data

U.S. DEPARTMENT OF ENERGY | Nuclear Energy

Oak Ridge National Laboratory

in partnership with

Electric Power Research Institute

Idaho National Laboratory

Los Alamos National Laboratory

Massachusetts Institute of Technology

North Carolina State University

Sandia National Laboratories

Tennessee Valley Authority

University of Michigan

Westinghouse Electric Company

and individual contributions from

Anatech Corporation
ASCOMP GmbH
CD-adapco, Inc
Core Physics, Inc.
City University of New York
Florida State University
Notre Dame University
Imperial College London
Pacific Northwest National Laboratory
Pennsylvania State University
Rensselaer Polytechnic Institute
Southern States Energy Board
Texas A&M University
University of Florida
University of Tennessee
University of Wisconsin

REVISION LOG

Revision	Date	Affected Sections	Revision Description
0	9/29/2014	All	Initial version

CONTENTS

ACRONYMS 2

1. Introduction 3

2. Transient Methods in MPACT 3

2.1 Transient Fixed Source Problem 3

2.2 CMFD Acceleration 7

3. Code Validation: SPERT 13

3.1. SPERT Description 13

3.2 MPACT Model 18

3.3 KENO Model 32

4. Results for SPERT Simulation 36

4.1 Steady State 36

4.2 Transient 43

5. Summary / Continuing Work 45

6. References 46

ACRONYMS

AMA	Advanced Modeling Applications
CASL	Consortium for Advanced Simulation of Light Water Reactors
CTF	COBRA-TF
DOE	U.S. Department of Energy
DOE-NE	U.S. Department of Energy Office of Nuclear Energy
DTK	Data Transfer Kit
FA	Focus Area
HFP	Hot Full Power
HPC	high-performance computing
HZP	Hot Zero Power
LWR	light water reactor
ORNL	Oak Ridge National Laboratory
PCI	pellet-cladding interaction
PCM	percent mille (10^{-5})
PPM	parts per million (usually boron)
PSU	Pennsylvania State University
PWR	pressurized water reactor
RTM	Radiation Transport Methods
SNL	Sandia National Laboratories
T-H	thermal-hydraulics
TPL	third-party library
V&V	verification and validation
VERA	Virtual Environment for Reactor Applications

1. Introduction

This report documents the second phase in the development, implementation, testing, and validation of the software modules in the MPACT neutron transport component required for a demonstrable transient capability necessary to support accident (e.g. RIA) scenarios. This work is a continuation of the first phase of the implementation which was reported in L3.RTM.SUP.P8.02 on March 31, 2014.

The following section will describe the transient methods implemented in MPACT which were modified slightly from those described in the March 31 report. Section 2 will then describe the steady-state and transient using the SPERT III E-Core for which some preliminary results were shown in the March 31 report. Continuing work is then discussed in Section 4.

2. Transient Methods in MPACT

2.1 Transient Fixed Source Problem

In order to determine the time-dependent pin-resolved power distribution, the transient calculation in MPACT is performed based on flat source region rather than CMFD coarse mesh. For this, the 3-D problem domain is first divided into several thick planes and radial flux distribution is solved by 2D MOC method. The axial coupling is resolved by one-dimensional (1-D) diffusion solutions and the planar and axial problems are coupled through the transverse leakage. The use of a lower order 1-D solution in the axial direction is justified by the fact that most heterogeneity in the core occurs in the radial direction rather than the axial. 3-D coarse mesh finite difference (CMFD) formulation is developed and used to accelerate the 2D radial and 1D axial solution. In the following section, the derivation of the MPACT transient solution method begins with the formulation of the multi-group MOC transient fixed source problem (TFSP) which involves the time discretization based on the theta method and precursor integration technique.

Then the formulation of CMFD method is introduced. Two different CMFD iteration schemes are developed and implemented. The 1G CMFD method updates the transient source based on the new coarse mesh flux and fission source and it needs multiple iterations until the transient source and fission source are converged. The MG CMFD method adds the transient source into the CMFD matrix and solves the whole matrix in one iteration.

Finally, a two-node NEM kernel is presented. Second order polynomial is used to approximate the transient source term. Due to the same order of polynomial approximation, the steady state NEM method is simply modified by adding transient source into the radial transverse leakage term to work with the transient formula.

Formulation of 2D MOC Transient Fixed Source Problem

The time dependent form of the planar transport problem which is obtained after integration of the angularly discretized 3-D Boltzmann transport equation can be written as follows for angle *m*:

$$\frac{1}{v_g}\frac{\partial \varphi_g^m}{\partial t}+\left(\eta_m\frac{\partial \varphi_g^m}{\partial x}+\varepsilon_m\frac{\partial \varphi_g^m}{\partial y}+\Sigma_{tg}\varphi_g^m\right)=\frac{1}{4\pi}\left(\chi_{pg}(1-\beta)\psi+\chi_{dg}S_d+\sum_{g'=1}^{G}\Sigma_{gg'}\phi_{g'}\right)$$
$$-\frac{\mu_m}{h_z}\left(\varphi_{gT}^m-\varphi_{gB}^m\right) \qquad (2\text{-}1)$$

where φ_g^m, ϕ_g, ψ, and S_d are the angular flux of angle *m*, scalar flux, total fission source, and delayed neutron source respectively, which are all axially averaged, whereas φ_{gT}^m and φ_{gB}^m are the angular fluxes at the top and bottom of the plane.

In addition, six more precursor equations are described below:

$$\frac{dC_k}{dt}=\beta\,\psi\;-\lambda_k C_k, k=1,2,...,6 \qquad (2\text{-}2)$$

where C_k is the delayed neutron precursor density, and ψ and S_d are the total fission source and the delayed neutron source defined as:

$$\psi\;=\sum_{g=1}^{G}\nu\Sigma_{fg}\phi_g\;, \qquad (2\text{-}3)$$

$$S_d=\sum_{k=1}^{K}\lambda_k C_k\;. \qquad (2\text{-}4)$$

In the above equations, the ν value is adjusted by the eigenvalue determined in the initial steady-state calculation.

For a given time step size Δt_n at time step *n*, Eq. (2-1) can be discretized using the theta method as:

$$\frac{\varphi_g^{m,n}-\varphi_g^{m,n-1}}{v_g^m\Delta t_n}=\theta\,R_g^{m,n}+(1-\theta)R_g^{m,n-1} \qquad (2\text{-}5)$$

with $R_g^{m,n}$ denoting all the right hand side terms of Eq. (2-1) at time step *n*. Eq. (2-5) can be rewritten as follows after dividing by θ:

$$\frac{\varphi_g^{m,n}}{\theta v_g^m\Delta t_n}-R_g^{m,n}=\frac{\varphi_g^{m,n-1}}{\theta v_g^m\Delta t_n}+\Theta R_g^{m,n-1} \qquad (2\text{-}6)$$

where $\Theta = \frac{1}{\theta} - 1$ is 1.0 for the Crank-Nicholsen scheme ($\theta = 0.5$) or 0.0 for the fully implicit scheme ($\theta = 1.0$). The RHS terms of Eq. (2-6) are all known from the solution of the previous time step and the flux at the current time step is the unknown to be determined.

Eq. (2-6) cannot be solved unless time differencing is performed to the precursor balance equation since the $R_g^{m,n}$ term contains the delayed neutron source term which involves the unknown delayed neutron precursor concentrations at time step *n*. In order to avoid the time differencing of the precursor equation, one can eliminate the unknown precursor term C_k^n from $R_g^{m,n}$ by introducing the second order precursor integration technique [Ref. 5] which is based on the second order variation of the fission source during the current time step. As a result, the delayed neutron source can be expressed as:

$$S_d^n = \sum_{k=1}^{K} \lambda_k C_k^{n-1} e^{-\lambda_k \Delta t_n} + \sum_{l=n-2}^{n} \sum_{k=1}^{K} \beta_k \Omega_k^l \psi^l \equiv \tilde{S}_d^{n-1} + \omega^n \psi^n \qquad (2\text{-}7)$$

where

$$\Omega_k^{n-2} = \frac{1}{\lambda_k \Delta t_{n-1}(\gamma+1)} \left(\frac{2(1-\kappa_k)}{\lambda_k \Delta_{t_{n-1}}} - \gamma(\kappa_k + 1) \right),$$

$$\Omega_k^{n-1} = \frac{1}{\lambda_k \Delta t_{n-1}} \left(\kappa_k + 1 + \frac{1-\kappa_k}{\gamma} \left(1 - \frac{2}{\lambda_k \Delta t_{n-1}} \right) \right) - \kappa_k ,$$

$$\Omega_k^{n} = 1 - \frac{2}{(\gamma+1)\lambda_k \Delta t_{n-1}} + \frac{1-\kappa_k}{\gamma(\gamma+1)\lambda_k \Delta t_{n-1}} \left(\frac{2}{\lambda_k \Delta t_{n-1}} - 1 \right),$$

$$\tilde{S}_d^{n-1} = \sum_{k=1}^{K} \kappa_k \lambda_k C_k^{n-1} + \sum_{l=n-2}^{n-1} \sum_{k=1}^{K} \beta_k \Omega_k^l \psi^l \qquad (2\text{-}8)$$

and

$$\omega^n = \sum_{k=1}^{K} \beta_k \Omega_k^n . \qquad (2\text{-}9)$$

with $\kappa_k = e^{-\lambda_k \Delta t_n}$ and $\gamma = \frac{\Delta t_n}{\Delta t_{n-1}}$.

By inserting the delayed neutron source terms determined by the previous time step values, Eq. (2-8), into Eq. (2-6) and expressing all the terms of $R_g^{m,n}$ explicitly, one can obtain the following transient fixed source problem:

$$\left(\eta_m \frac{\partial \varphi_g^{m,n}}{\partial x} + \varepsilon_m \frac{\partial \varphi_g^{m,n}}{\partial y}\right) + \left(\Sigma_{tg} + \frac{1}{\theta v_g \Delta t_n}\right)\varphi_g^{m,n}$$
$$= \frac{1}{4\pi}\left(\left(\chi_{pg}(1-\beta) + \chi_{dg}\omega\right)\psi^n + \sum_{g'=1}^{G}\Sigma_{gg'}\phi_{g'}^n\right) \tag{2-10}$$
$$-\frac{\mu_m}{h_z}\left(\varphi_{gT}^m - \varphi_{gB}^m\right) + \frac{\varphi_g^{m,n-1}}{\theta v_g \Delta t_n} + \frac{1}{4\pi}\chi_{dg}\tilde{S}_d^{n-1} + \Theta R_g^{m,n-1}$$

Here the residual term appearing last represents the imbalance between neutron production and loss in direction *m* at a point. In principle, Eq. (2-10) can be solved by MOC as long as the RHS is exactly known for each flat source region. However, there are several practical difficulties in solving Eq. (2-10). First of all, the total cross section is augmented by the 1-over-vΔt term. This augmentation changes the ray attenuation characteristics in the MOC solution since all the exponential terms have to be evaluated with the augmented cross section. Secondly, since the angular flux of the previous step appears on the RHS, all the angular flux should be stored at every flat source region which would cause a significant increase in the memory.

In order to avoid these problems, the 1-over-vΔt term of the current time step is first moved to the RHS so that the left hand side becomes identical to the steady-state form. The angular dependence of the 1-over-vΔt term is then neglected by treating this term isotropic. This approximation would have negligible impact since the isotropy assumption is applied to the difference term not to the angular flux itself. Furthermore the angular dependence of the residual term is neglected. Eq. (2-10) now becomes

$$\left(\eta_m \frac{\partial \phi_g^{m,n}}{\partial x} + \varepsilon_m \frac{\partial \phi_g^{m,n}}{\partial y}\right) + \Sigma_{tg}\phi_g^{m,n} = \frac{1}{4\pi}\left(\left(\chi_{pg}(1-\beta) + \chi_{dg}\omega\right)\psi^n + \sum_{g'=1}^{G}\Sigma_{gg'}\varphi_{g'}^n\right)$$
$$-\frac{\mu_m}{h_z}\left(\phi_{gT}^m - \phi_{gB}^m\right) + \frac{1}{4\pi}\left(\chi_{dg}\tilde{S}_d^{n-1} + \Theta R_g^{n-1} - \frac{\varphi_g^n - \varphi_g^{n-1}}{\theta v_g \Delta t_n}\right) \tag{2-11}$$

Once the delayed neutron source and the residual terms are given for each flat source region, Eq. (2-11) can be solved using the steady-state MOC solver with only a few additions of source terms. The final equation becomes:

$$\left(\eta_m \frac{\partial \varphi_g^{m,n}}{\partial x} + \varepsilon_m \frac{\partial \varphi_g^{m,n}}{\partial y}\right) + \Sigma_{tg}\varphi_g^{m,n}$$
$$= \frac{1}{4\pi}\left(\chi_g\psi^n + \sum_{g'=1}^{G}\Sigma_{gg'}\phi_{g'}^n\right) - \frac{\mu_m}{h_z}\left(\varphi_{gT}^m - \varphi_{gB}^m\right) + \frac{1}{4\pi}S_{tr}^{g,n}, \tag{2-12}$$

where the transient specific source is defined as:

$$S_{tr}^{g,n} = \left(\chi_{pg}(1-\beta) + \chi_{dg}\omega - \chi_g\right)\psi^n + \chi_{dg}\tilde{S}_d^{n-1} + \Theta R_g^{n-1} - \frac{\varphi_g^n - \varphi_g^{n-1}}{\theta v_g \Delta t_n}. \qquad (2\text{-}13)$$

In order to work with CMFD acceleration and nodal NEM method, the transient source is rearranged as below:

$$\begin{aligned} S_{tr}^{g,n} &= -\frac{\varphi_g^n}{\theta v_g \Delta t_n} + \left(\chi_{pg}(1-\beta) + \chi_{dg}\omega - \chi_g\right)\psi^n + \chi_{dg}\tilde{S}_d^{n-1} + \Theta R_g^{n-1} + \frac{\varphi_g^{n-1}}{\theta v_g \Delta t_n} \\ &= A\varphi_g^n + B\psi^n + C \end{aligned} \qquad (2\text{-}14)$$

Where A and B are flux and fission source dependent term, while C is a constant term:

$$\begin{aligned} A &= -\frac{1}{\theta v_g \Delta t_n} \\ B &= \left(\chi_{pg}(1-\beta) + \chi_{dg}\omega - \chi_g\right) \\ C &= \chi_{dg}\tilde{S}_d^{n-1} + \Theta R_g^{n-1} + \frac{\varphi_g^{n-1}}{\theta v_g \Delta t_n} \end{aligned} \qquad (2\text{-}15)$$

2.2 Coarse mesh finite difference (CMFD) acceleration

Two types of CMFD acceleration methods are developed in MPACT for transient calculation, 1G (1 group) CMFD and MG(multi-group) CMFD. MG CMFD is recommended since it formulates the entire CMFD matrix and is solved in one iteration, which runs much faster than 1G CMFD.

Similar to MOC equation, the CMFD based neutron balance equation can be easily formulated by adding a transient source term. The transient source in the equation is CMFD coarse mesh based and is homogenized from flat source fine mesh.

$$\sum_{u=x,y,z} \frac{1}{h_u^m}\left(J_{gu}^{m+} - J_{gu}^{m-}\right) + \Sigma_{rg}^m \phi_g^{m,n} = \chi_g \psi^m + \sum_{\substack{g'=1 \\ g'\neq g}}^{G} \Sigma_{gg'}^m \phi_{g'}^{m,n} + S_{tr}^{m,n} \qquad (2\text{-}16)$$

Instead of homogenizing the fine mesh transient source term, the transient source coefficient *A*, *B* and *C* are homogenized by the following equation:

$$A_g^m = \frac{\sum_{i=1}^{I^m} A_g^{m,i}\varphi_g^{m,i}V^{m,i}}{\sum_{i=1}^{I^m} \varphi_g^{m,i}V^{m,i}}, B^m = \frac{\sum_{i=1}^{I^m} B^{m,i}\psi^{m,i}V^{m,i}}{\sum_{i=1}^{I^m} \psi^{m,i}V^{m,i}}, C^m = \frac{\sum_{i=1}^{I^m} C^{m,i}V^{m,i}}{\sum_{i=1}^{I^m} V^{m,i}} \qquad (2\text{-}17)$$

As a result, the CMFD transient source can be update by new CMFD flux and fission source.

$$S_{tr,g}^{m,n} = A_g^m \phi_g^n + B^m \psi^n + C^m \tag{2-18}$$

The 1G CMFD acceleration technique is similar to traditional steady state CMFD acceleration technique, while 1G transient CMFD does not need to update eigenvalue for each CMFD iteration. In each CMFD iteration, the transient source is updated using the new calculated CMFD flux and fission source using equation (2-18) and added to the right hand side term as source. The steady state CMFD then be used to calculate the transient CMFD fixed source problem. The flow chart is shown in Fig. 2-1. One disadvantage of this method is that it needs multiple CMFD iterations to converge before one MOC solve and the number of iteration is tremendously large for transient problem with large power change since the right hand side (fission source and transient source) changes dramatically during a transient step.

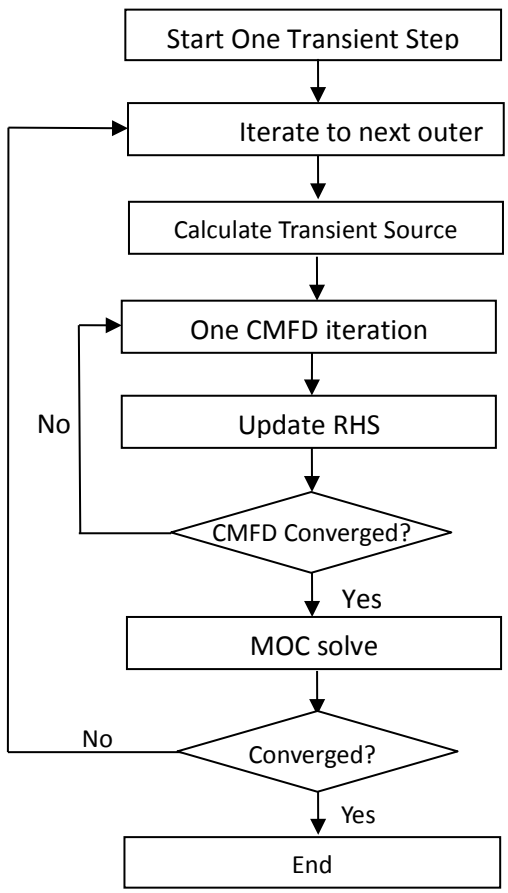

Figure 2-1 One-Group CMFD flow chart

In order to solve the slow converging problem in 1G CMFD, MG CMFD method is developed. The basic idea of this method is to add transient source coefficient into the whole CMFD matrix and solve the whole matrix in one iteration. Different from steady state eigenvalue calculation, transient calculation does not need to update eigenvalue during one transient step. As a result, the CMFD flux dependent source (including transient source and fission source) at right hand side in the transient matrix can be moved to the left hand side and then the matrix can be solved in one iteration.

The following notations are used to present the matrix operations:

- Removal term: $\mathbf{M} = -\nabla \mathbf{D} \nabla + \mathbf{xsT}$
- Scattering: $\mathbf{S} = \mathbf{xsS}$
- Fission source: $\mathbf{F} = \mathbf{chi} * \mathbf{xsNF} / k_{eff}$
- The transient source is defined in equation (3-3) is : $\mathbf{S}_{tr} = \mathbf{A} * \phi + \mathbf{B} * \mathbf{F} * \phi + \mathbf{C}$

The neutron balance equation for MG CMFD is:

$$(\mathbf{M} - \mathbf{S}) * \phi = \mathbf{F} * \phi + \mathbf{A} * \phi + \mathbf{B} * \mathbf{F} * \phi + \mathbf{C} \qquad (2\text{-}19)$$

Remove the flux dependent term from right hand side to the left hand side, it becomes:

$$(\mathbf{M} - \mathbf{S} - \mathbf{F} - \mathbf{A} - \mathbf{B} * \mathbf{F}) * \phi = \mathbf{C} \qquad (2\text{-}20)$$

The above equation is a standard linear system and the unknown flux can be solved simultaneously by any matrix inverse method in one iteration. Another advantage of this method is the unknown flux calculated by the MG CMFD is fully converged while the 1G CMFD only converges to the convergence criteria specified by user input, which is usually 1E-4.

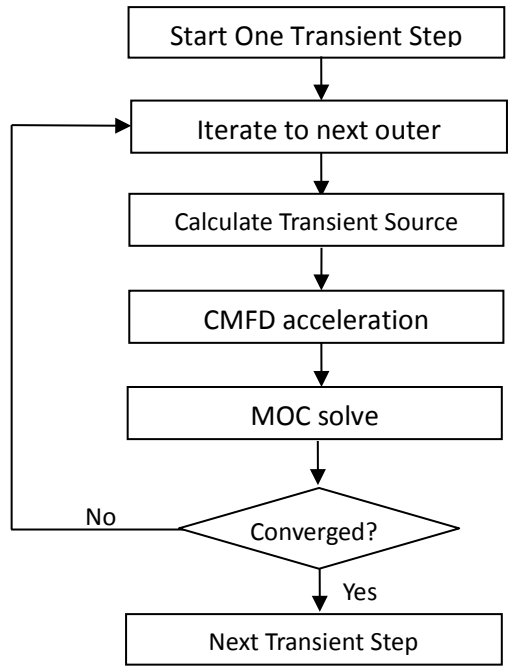

Figure 1-2 Multi-Group CMFD flow chart

Transient Two-Node NEM Formulation

The TFSP of Eq. (2-12) contains the axial net current which is to be determined by the NEM. Specifically, the net current is solved for the given incoming current boundary condition specified at the top and bottom surfaces of the node. In order to derive an expression that represents the net current in terms of the incoming partial current and the node average flux, the one-dimensional, one-group continuous form of the TFSP is written as follows:

$$-D\frac{d^2\phi_g^n(z)}{dz^2}+\Sigma_{rg}\phi_g^n(z)=-L_R^n(z)+\chi_g\psi^n(z)+\sum_{\substack{g'=1\\g'\neq g}}^{G}\Sigma_{gg'}^m\phi_{g'}^n(z)+S_{tr}^{g,n}(z) \qquad (2\text{-}21)$$

where the radial transverse leakage is defined as:

$$L_R^n(z)=\sum_{u=x,y}\frac{1}{h_u}\left(J_{gu}^{n+}(z)-J_{gu}^{n-}(z)\right) \qquad (2\text{-}22)$$

and the transient source is defined as:

$$S_{tr}^{n}(z) = \left(\chi_{pg}(1-\beta^{n}) + \chi_{dg}\omega^{n} - \chi_{g}\right)\psi^{n}(z) + \chi_{dg}\tilde{S}_{d}^{n-1}(z) + \Theta R_{g}^{n-1}(z) - \frac{\varphi_{g}^{n}(z) - \varphi_{g}^{n-1}(z)}{\theta v_{g}^{m}\Delta t_{n}} \quad (2\text{-}23)$$

It is assumed here that the fission source and fluxes of the other groups as well as the last three terms originating from the previous time step are all known and the incoming currents are specified at the top and bottom surfaces of the node.

In principle, the steady state NEM equation can be solved by employing the fourth order polynomial expansion for flux, second order polynomial for the transverse leakage term and fourth order polynomial for the fissions source term. The detailed expressions for the coefficients are not given here.

In order to work with equation (2-21), a second order polynomial expansion is used to approximate the transient source term:

$$hS_{tr}^{n}(\xi) = \sum_{k=0}^{2} s_{tr,k} P_{k}(\xi) \quad (2\text{-}24)$$

Where $P_0(\xi) = 1,\ P_1(\xi) = \xi,\ P_2(\xi) = \frac{1}{2}(3\xi^2 - 1)$

The transient source moment is calculated as follows:

$$\begin{aligned}
s_{tr,0} &= h^{c} S_{tr}^{c} \\
s_{tr,1} &= G^{-1}\left(h^{c}\right)^{2}\left[(S_{tr}^{r} - S_{tr}^{c})(h^{c} + 2h^{l})(h^{c} + h^{l}) - (S_{tr}^{l} - S_{tr}^{c})(h^{c} + 2h^{r})(h^{c} + h^{r})\right] \\
s_{tr,2} &= G^{-1}\left(h^{c}\right)^{3}\left[(S_{tr}^{r} - S_{tr}^{c})(h^{c} + h^{l}) + (S_{tr}^{l} - S_{tr}^{c})(h^{c} + h^{r})\right] \\
G &= 2(h^{c} + h^{l})(h^{c} + h^{r})(h^{c} + h^{l} + h^{r})
\end{aligned} \quad (2\text{-}25)$$

$s_{tr,0}$, $s_{tr,1}$ and $s_{tr,2}$ are 0th, 1st, and 2nd transient source moments, S_{tr} is the average transient source in the node and h is the length of the node. The superscript *c*, *l* and *r* denote the current, left and right node. Due to the use of a second order approximation of the transient source which is identical to the treatment of the radial transverse leakage term, the NEM solver used for the steady-state calculation can be used almost directly by adding the transient source term into transverse leakage term.

Iteration Strategy

The flow chart of the MPACT transient algorithm is shown below:

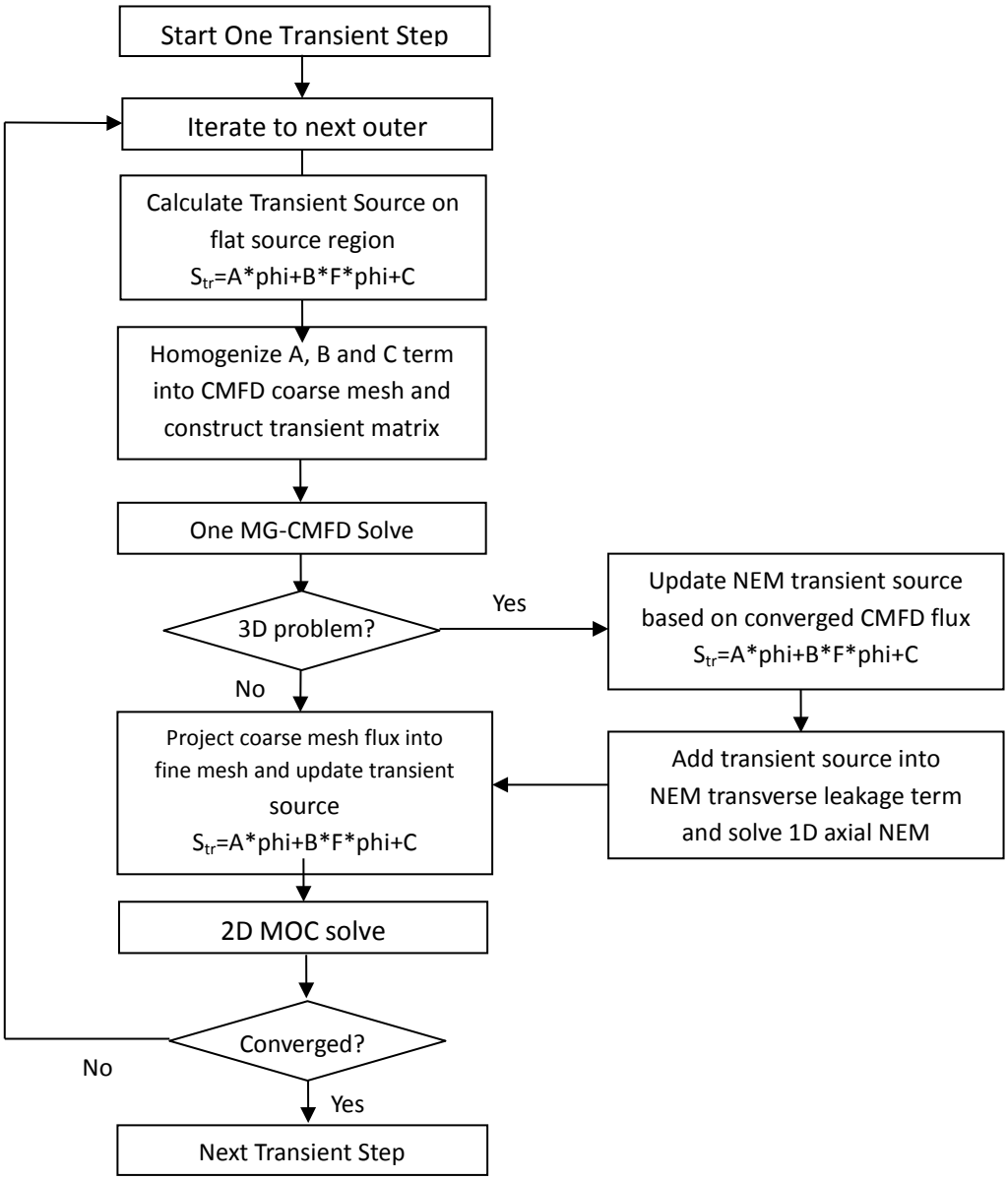

Figure 2-2 MPACT transient iteration scheme

3. Code Validation: SPERT

Pin resolved, three-dimensional neutron transport modeling of the reactor core has become increasing important for a range of multi-physics applications. The verification and validation (V&V) of these methods, however, is a considerable challenge because of the lack of sufficiently detailed experimental data for power reactor conditions, particularly for transient conditions. One of the most frequently used experiments for transient validation has been the Special Power Excursion Reactor Test (SPERT) project which was established as part of the U. S. Atomic Energy Commission's reactor safety program in 1954.

The SPERT project was designed to investigate the kinetic behavior of nuclear reactors subjected to large positive reactivity insertions. The SPERT III reactor (Durgone, 1965) was a pressurized water nuclear reactor designed to incorporate the essential features of pressurized-water and boiling-water reactors. General objectives in the SPERT III facility were to (a) to provide a facility in which reactor power excursion tests could be performed and experimental information gathered on the kinetic behavior of the reactor, (b) to incorporate in the design a complete reactor and coolant system typical of existing and proposed pressurized water power reactors to permit an investigation of safety problems common to this class of reactors, and (c) to incorporate sufficient flexibility in the overall design to permit studies on several core designs. Among several core designs, the E-Core consisting of 60 assemblies was employed to perform some reactivity insertion accident (RIA) experiments. The data measured during the E-Core experiments was used here to validate the neutronics performance of the MPACT code for both steady-state and transient conditions.

The SPERT III E-Core has been used previously by several researchers to validate transient computer codes to include CASMO/SIMULATE-3K of Studsvik Scandpower Inc. (Grandi, 2012), ANCK/MIDAC code of Westinghouse (Aoki et al., 2009), and the SCALE/PARCS code system of the U.S. NRC (Wang, 2013). While most of the work has been devoted to simulation of its transient behavior, the steady-state has not been well analyzed. CASMO5/SIMULATE-3K has been validated against SPERT III E-Core at cold startup measurements (Grandi, 2012). In most all cases, a significant discrepancy was observed in the predicted and measured critical control rod position at cold zero power (CZP). All of these relied upon coarse mesh nodal methods using homogenized cross sections which do not explicitly model the complex geometry of the core.

The MPACT (Michigan Parallel Characteristics based Transport) code used in the work here was developed by the University of Michigan to perform whole core pin resolved LWR analysis without homogenization (Kochunas, 2013). The SPERT validation of MPACT was supplemented by use of the Monte Carlo code KENO V.a which is part of the SCALE code package (Bowman, 2011). Both KENO and MPACT are able to explicitly model the complex geometry of SPERT-III E-Core core without homogenization. An objective of the KENO comparison was to identify the important details of the SPERT model required to build confidence in the steady-state three-dimensional MPACT model of the reactor.

3.1 SPERT III E-core Description

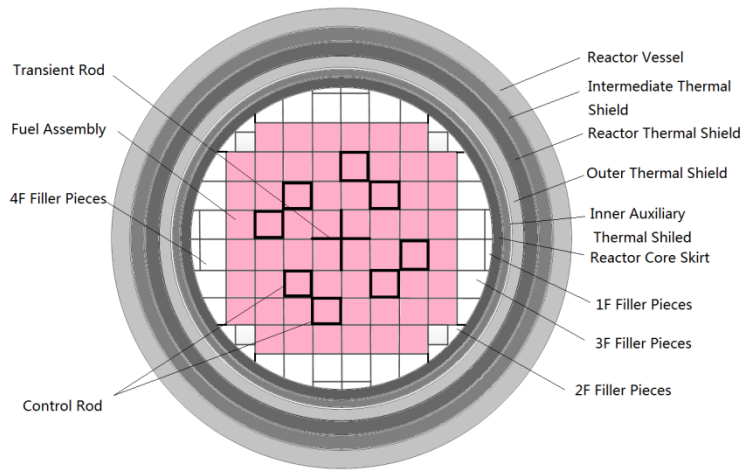

Figure 3-1 SPERT III E-core cross-section.

Some of the basic data on the SPERT III E-core is listed in Table . A more complete listing of Reactor Component Design Data is provided in Appendix A.

Table 3-1 Basic Core / Fuel Data for SPERT III E-core

Parameters	Value
Reactor Type	Experimental PWR
Moderator/Coolant	H_2O/H_2O
Core Power	20 MW
Core equivalent diameter	0.66 m
Active height	97.282 cm
Fuel rod outer diameter	1.1836 cm
Fuel rod inner dimeter	1.0820 cm

Fuel pellet diameter	1.0668 cm
Fuel rod pitch	1.4859 cm
Fuel enrichment	4.8 wt% enriched UO_2 (10.5 g/cm^3)
Fuel tube	Stainless steel, type 348
Gas gap	Helium
Control rods composition	Absorber section 1.35 wt% ^{10}B in Type 18-8 stainless steel; 0.4724 cm thick hollow square box
25 rod Fuel assembly	7.5565*7.5565*130.175 cm
16 rod Fuel assembly	6.3398*6.3398*130.175 cm
CR with fuel followers	6.2890*6.2890*112.673 cm
Fuel assembly pitch	7.62 cm
Filler pieces thickness	0.3175 cm
Assembly box thickness	0.3175 cm

The fuel rods are 40.8 inches long, excluding end plugs, by 0.466 inches in outside diameter with a wall thickness of 0.020 inches. The tubing and end plugs are composed of Types 348 and 347 stainless steel, respectively. The fuel is in the form of uranium dioxide pellets, 4.8 weight percent enriched, 0.420 inch in diameter. Each of the fuel rods contains 38.5 grams of U-235 with an active fuel length of 38.3 inches which leaves a 2.5-inch expansion space at the top of the fuel rod. In this expansion space, a compression spring is positioned to keep the fuel pellets in place. The gas in the fuel rods is 95 percent helium to improve the heat transfer across the gas gap.

The 25 fuel rods are spaced on a 0.585 inch square pitch in the fuel can by upper and lower fuel grids and two intermediate grids. The intermediate grids are spaced 13 inches and 26.5 inches above the lower fuel grid to minimize vibration and thermal bowing of the fuel rods. There is no clear description of the shape and weight of grids. A total area of 120 square inches in the form of slots has been removed from each stainless steel fuel can. These slots are so arranged that by proper orientation of the fuel assemblies, the slots in adjacent assemblies can be either aligned or blocked. The alignment of the slots allows core cross flow. The overall dimensions of the fuel assembly are 2.975 inches wide by 2.975 inches thick by 52.750 inches long. The average heat transfer surface, based on the active fuel length, is 1402 square inches per assembly, and the nonmoderator-to-moderator ratio is 1.03 for a 3-by 3-inch cell.

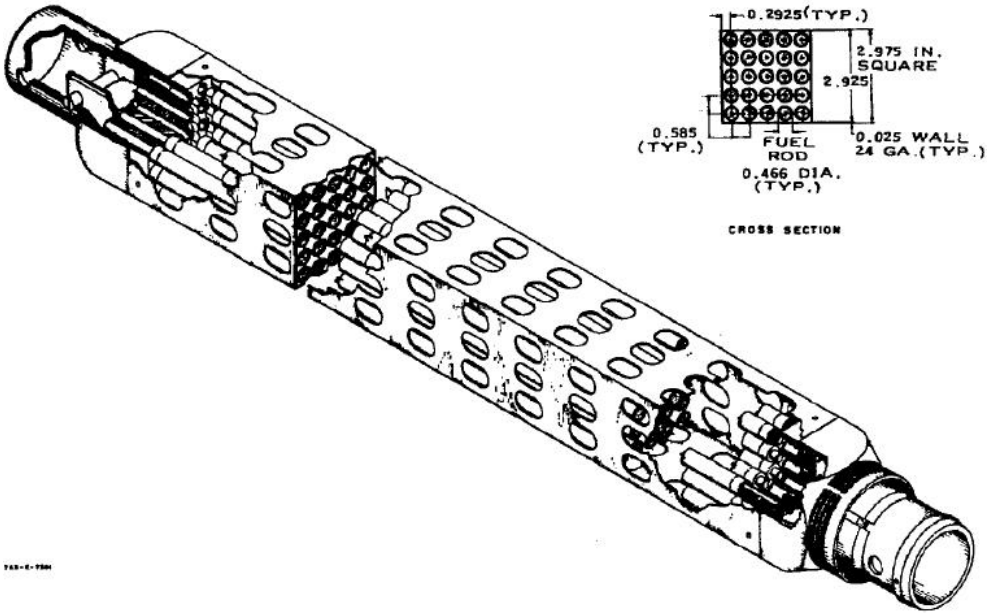

Figure 3-2: 25-rod Fuel Assembly

There are eight control rods located in the core, two of which are provided in each quadrant. The two rods are joined by a yoke and driven by a single drive mechanism. The rods are the fuel-poison type, containing fuel in the lower section and a poison (neutron absorber) material in the upper section. A control rod assembly is shown in Figure 3-3.

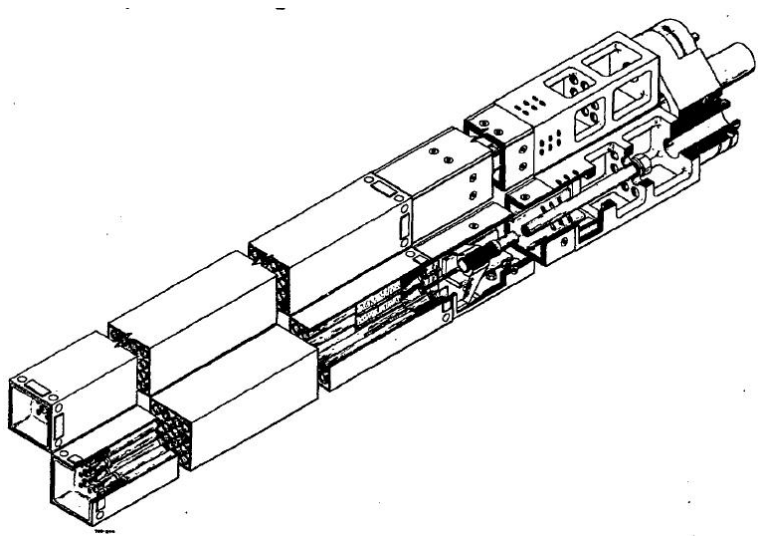

Figure 3-3: Control Rod Assemblies on one Yoke

The fuel section of the control rod assemblies consists of 16 fuel rods containing a total of 616 g of U-235. The fuel rods are the same as those used in the fuel assemblies. They are spaced on a 0.585 inch square pitch to give a flow area of 2.80 square inches. The average heat transfer area is 897 square inches per control rod, and the overall dimensions of the fuel section are 2.496 inches wide by 2.496 inches thick by 45.65 inches long. The poison section is a square box constructed of 0.186-inch-thick Type 18-8 stainless steel plate containing 1.35 weight percent boron-10. The overall dimensions of this section are 2.496 inches square by 46 inches long.

Flux suppressors are provided in the region between the end of the poison box and the top of the fuel rods. There are 12 suppressors in each control rod assembly. Six of the suppressors are 2.184- by 1- by 0.030-inch plates while the other six are 2.340- by 2-23/32- by 0.030-inch plates. These suppressors are made of the same material (boron-10 stainless steel alloy) as the poison section. However, there is no more detailed description on the structure of the flux suppressors.

The transient rod is a cruciform-shaped rod with blades 5.125 inches wide by 0.1875 inches thick. The upper section, which is normally in the core, is 56 inches long and constructed of 18-8 stainless steel. The lower section, which is the absorber section and normally extends below the core, is 38 inches long and constructed of 1.35 weight percent boron-10 stainless steel. The two sections are welded together and machined smooth. Haynes No. 40 alloy bushing pads, 4.625 inches square by 0.09 inches thick, guide and position each blade in the transient rod guide. The yoke section, constructed of 347 stainless steel, is pinned to the upper section of the rod and forms the coupling between the transient rod and transient rod drive. See 3-4 for the transient rod assembly.

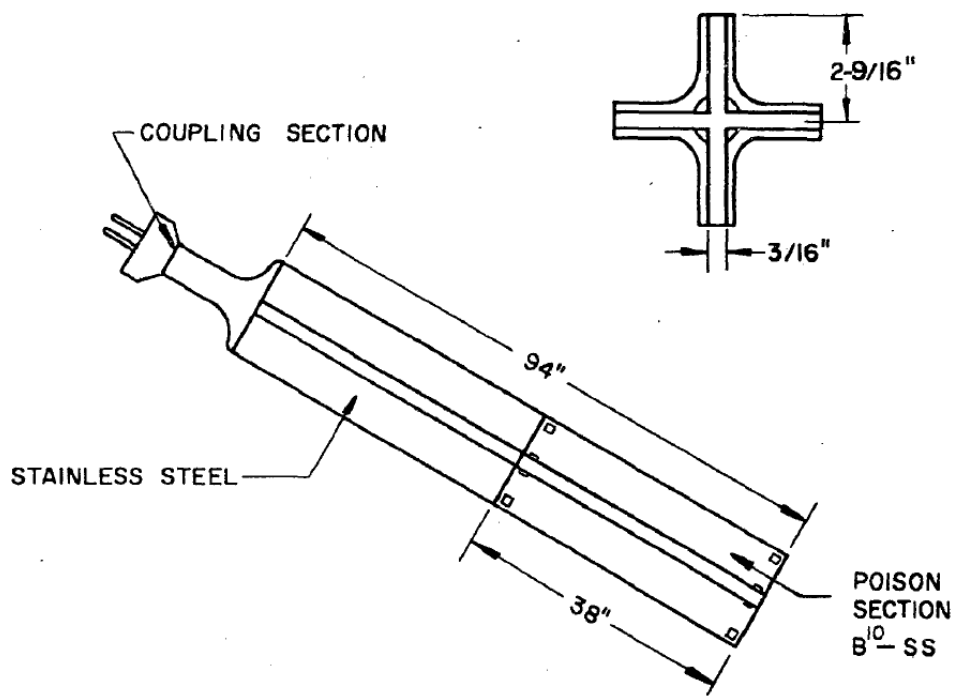

Figure 3-4: Transient rod assembly.

The 16-rod fuel assembly is similar to the 25-rod fuel assembly. The fuel rods and the fuel rod pitch are the same as the 25-rod fuel assembly. The assembly contains 16 fuel rods. The overall dimensions of the fuel assembly are 2.476 inches wide by 2.476 inches thick by 52.750 inches long. The average heat transfer surface is 897 square inches per assembly, and the nonmoderator-to-moderator ratio is 0.942 for the assembly.

Since the core skirt is cylindrical, the space between the square fuel assembly positions and the cylindrical core skirt must be occupied by appropriately shaped filler pieces. Dummy spacer assemblies (Filler pieces) of the shapes shown in Figure 3-5 are therefore required to fill the lattice positions unoccupied by fuel assemblies in order to maintain hydraulic equilibrium for various core sizes. These assemblies are designated as Type 1F, 2F, 3F and 4F respectively according to the space requirement. The filler box is constructed of 1/8-inch plate welding to the size and shape required.

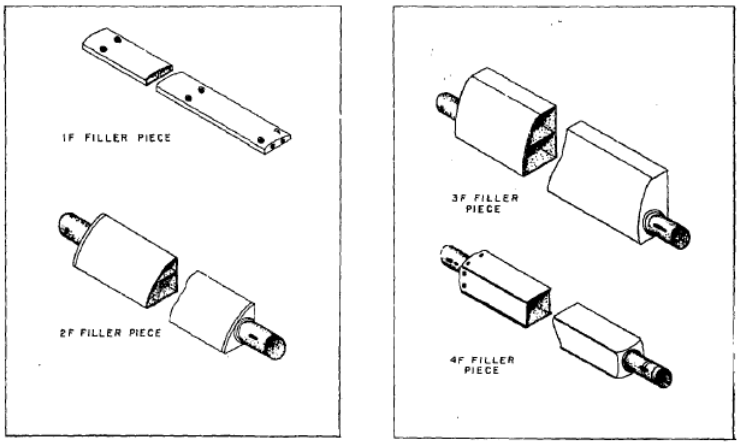

Fig. 11 1F and 2F filler pieces.

Fig. 12 3F and 4F filler pieces.

Figure 3-5: Core Filler Pieces

3.2 MPACT model of the SPERT III E-core

The fuel pin is modeled as in Figure 3-6. MPACT uses the “pin” as the unit of CMFD meshing. All “pins” must be arranged in a regular array. The fuel pins in the 25-rod assemblies and 16-rod assemblies have the same size and pin pitch but are offset by a half pitch. To meet the requirement of CMFD meshing, each fuel pin must be subdivided into four quarter pins.

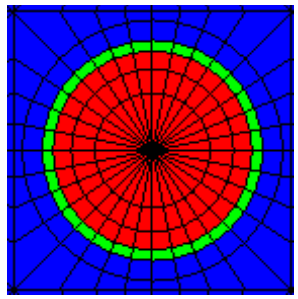

Figure 3-6: MPACT model of fuel pin

Each quarter pin is a 0.74295 cm (0.2925 inches) x 0.74295 cm square with 3 concentric arcs of material boundaries with the actual pin center at a corner of the "pin" mesh. The radius of the first (smallest) arc is 0.5334 cm (0.21 inches); the material within this arc is 4.8 percent enriched sintered UO_2 with a density of 10.5 g/cm^3. The radius of the second arc is 0.59182 cm (0.233 inches); the material between first and second arcs is a mixture of 87.545 volume percent type 348 stainless steel and 12.455 volume percent helium. The material outside of the second arc is all coolant. The coolant is un-borated water with varied temperature depending on the particular experiment. The third arc is added within the coolant region for improving discretization.

The 25-rod assembly is modeled as in Figure 3-7. The inner part of the 25-rod assembly model consists of 10 x 10 quarter fuel pins. This array is surround by a 0.0635 cm (0.025 inches) thick can and 0.03175 cm of bypass water outside the can. The can and bypass water together form one layer of MPACT "pins". Therefore, the 25-rod assembly is divided into a 12 x 12 array of "pin" meshes. The thicknesses of the inner "pin" meshes are 0.74295 cm, and thicknesses of the outer "pin" meshes are 0.09525 cm. This meshing will be used for all other assembly models.

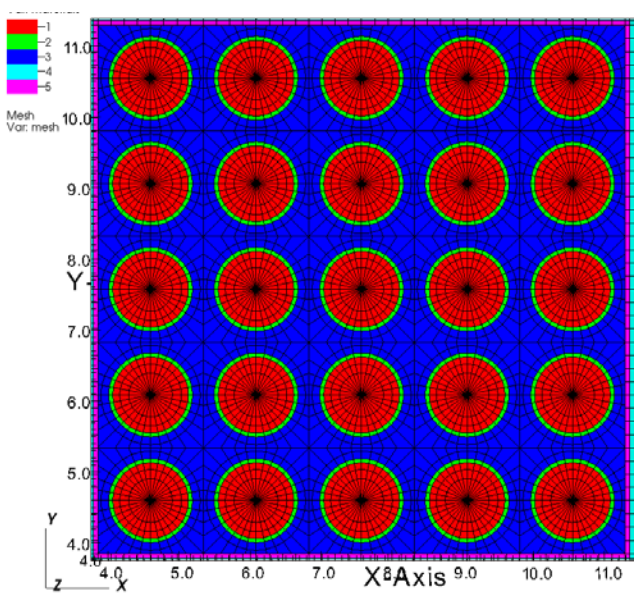

Figure 3-7: MPACT model of 25 rod assembly

The bypass gap is unheated, un-borated water; the temperature and density vary depending on the experiment. The can consists of a mixture of 75 volume percent stainless steel and 25 volume percent unheated water. The water is present to represent the 120 square inches of slots that has been removed from each stainless steel fuel can. The top part (absorber) of the control rod is modeled as in Figure 3-8 The outer dimension of absorber the is 6.28904 cm (2.476 inches) x 6.28904 cm. The thickness is 0.47244 cm (0.186 inches). The absorber is divided into two rings of MPACT "pin" meshes to match the meshing with the 25-rod assembly. The thickness of absorber in the outer ring of "pin" meshes is 0.19812 cm (0.078 inches), while the thickness of absorber in the inner ring of "pin" meshes is 0.27432 cm (0.108 inches).

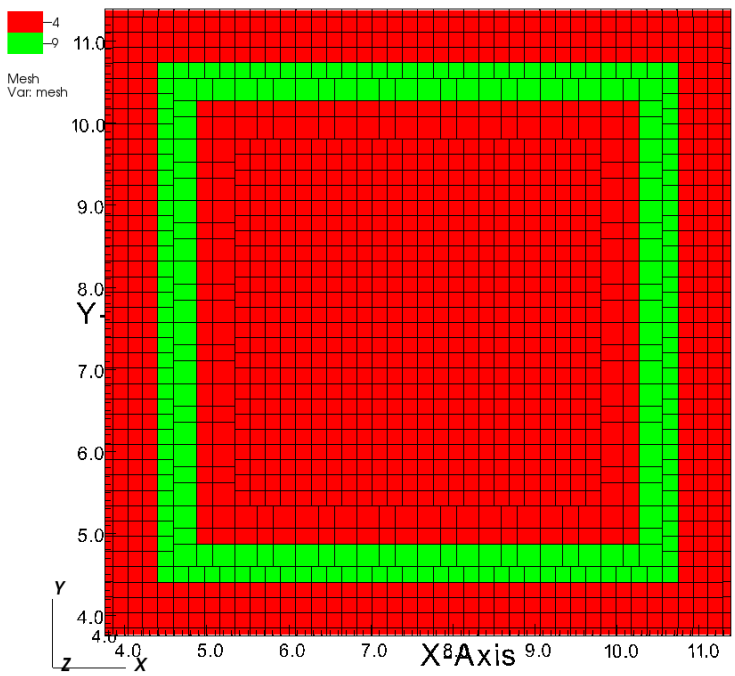

Figure 3-8: MPACT model of control rod

The control rod absorber consists of type 18-8 stainless steel plates containing 1.35 weight percent boron-10. The remaining material in the control rod model (both inside and outside the absorber) is unheated un-borated water.

The control rod follower is modeled as in Figure 3-9. There is an 8 x 8 array of quarter pins at the center of the assembly. This is surrounded by the can for the follower, located within the ring of "pin" meshes surrounding the fuel pins. The thickness of the can is 0.183701191 cm (0.072323 inches), which is calculated from 2.80 square inches of flow area. There is a 0.014419 cm (0.005677 inches) gap between the can and the 8 x 8 array of quarter pins.

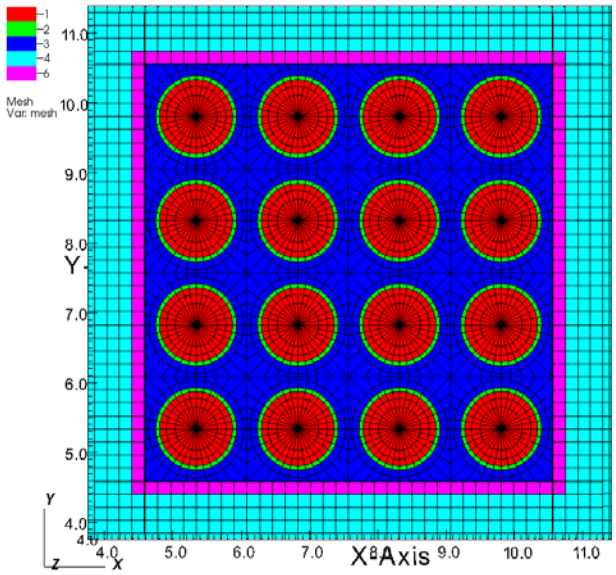

Figure 3-9: MPACT model of control rod follower

The can consists of stainless steel, and the material in the gap between the can and the 8 x 8 array of quarter pins is un-borated water, while the material outside of the can is unheated un-borated water.

The 16–rod assembly surrounded by one quarter of the cruciform transient rod on two sides is modeled as in Figure 3-10. There is an 8 x 8 array of quarter pins at the center of the assembly, which is identical to the control rod follower. Also like the control rod follower, the can is located within the ring of “pin” meshes surround the fuel pins. The thickness of the can is 0.0635 cm (0.025 inches), which is calculated from the 3.16 square inches of flow area and a nonmoderator-to-moderator ratio of 0.942. There is a 0.10922 cm (0.043 inches) gap between the can and the 8 x 8 array of quarter pins. There is a control rod blade in one corner of the assembly extending along two sides. The thickness of the blade in the model is 0.238125 cm (3/32 inches), corresponding to half of the thickness of the cruciform-shaped transient rod blades. As the thickness of the peripheral cell is 0.09525 cm (0.0375 inches), the rest of control blade, with a thickness of 0.142875 cm (0.05625 inches), is located in the second outer ring of “pin” meshes together with the can. There are four different material regions in the “pin” mesh from outside in: 0.142875 cm (0.05625 inches) of control blade, 0.427355 cm (0.16825 inches) of bypass water, the 0.0635 cm (0.025 inches) thick can and 0.10922 cm (0.043 inches) of coolant region. The blade length is 2.0625 inches, which extends to the last row of “pin” meshes with quarter fuel pins. The length of the blade in the last cell is 0.6858 cm (0.27 inches).

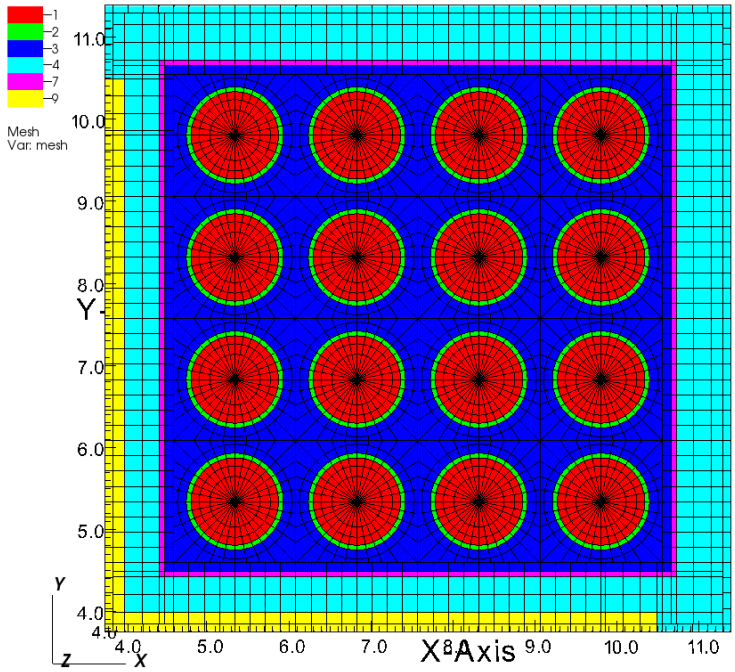

Figure 3-10: MPACT model of 4x4 assembly with cruciform transient rod

The can is composed of stainless steel, and the control blade is composed of type 18-8 stainless steel plate containing 1.35 weight percent boron-10. The material in the gap between the can and the 8 x 8 array of quarter pins is un-borated water, while the material outside of the can is unheated un-borated water. When the control blade is withdrawn, the model is the same as shown in Figure except the control blade material is replaced by stainless steel without boron. There are three other quarters of the transient rod surrounding 16–rod assemblies that are identical to in Figure except rotated.

The core filler pieces are explicitly model in MPACT as shown in Figure 3-11. The thickness of the filler box is 0.3175 cm (1/8 inches) and the outer dimension is the same as the 25-rod fuel assembly. The curved portion of type 1F, 2F and 3F are approximated on the rectangular grid.

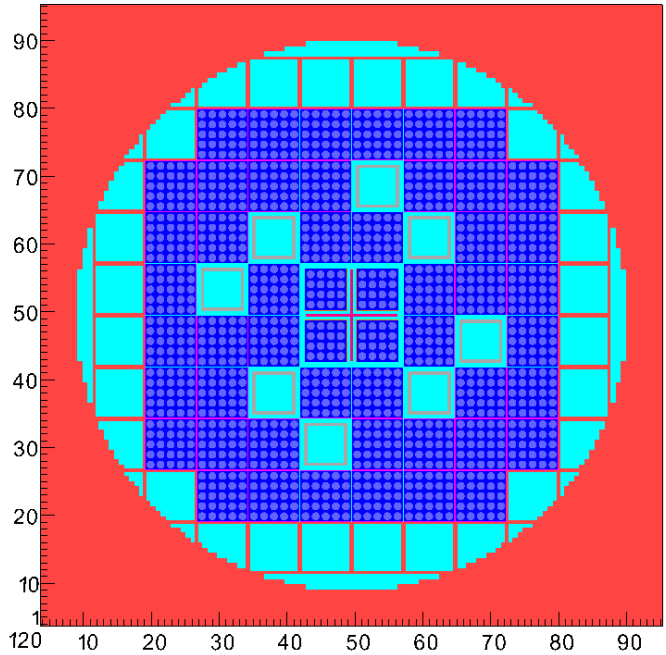

Figure 3-11: MPACT model for core filler

The weight of the intermediate grids is not provided in the SPERT-III documentation, so the weight of one grid is estimated to be 300 grams. Because the structure of the grid is too complex to model explicitly, it is homogenized with the coolant in a height of approximately 6 cm. The corresponding volume fraction of steel and water is 19% and 81%, respectively. The position of the two axial grids are the in the 6th and the 12th node from the bottom of the active core.

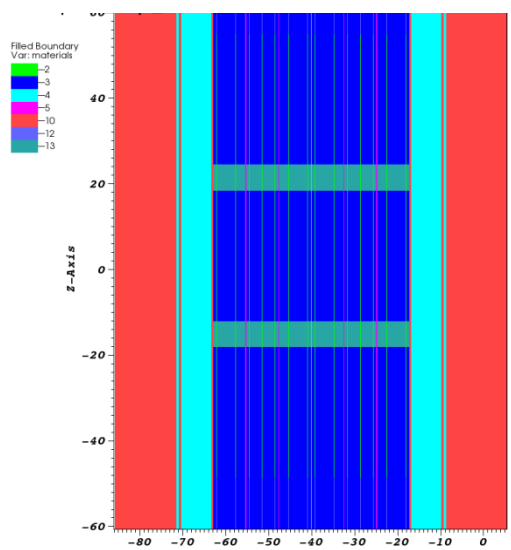

Figure 3-12: MPACT model for axial grids

The flux suppressors between the control rod absorbers and fuel followers are modeled. According to the reference, the distance between the absorber and fuel follower is 4.7 inches, so the lower half of that height is filled with spring like the other fuel rods, while the upper half is filled with moderator and type 18-8 stainless steel containing 1.35 weight percent of boron-10. While the precise geometry of the flux suppressor is not available, the volume of steel containing boron-10 is preserved with the data given in the document.

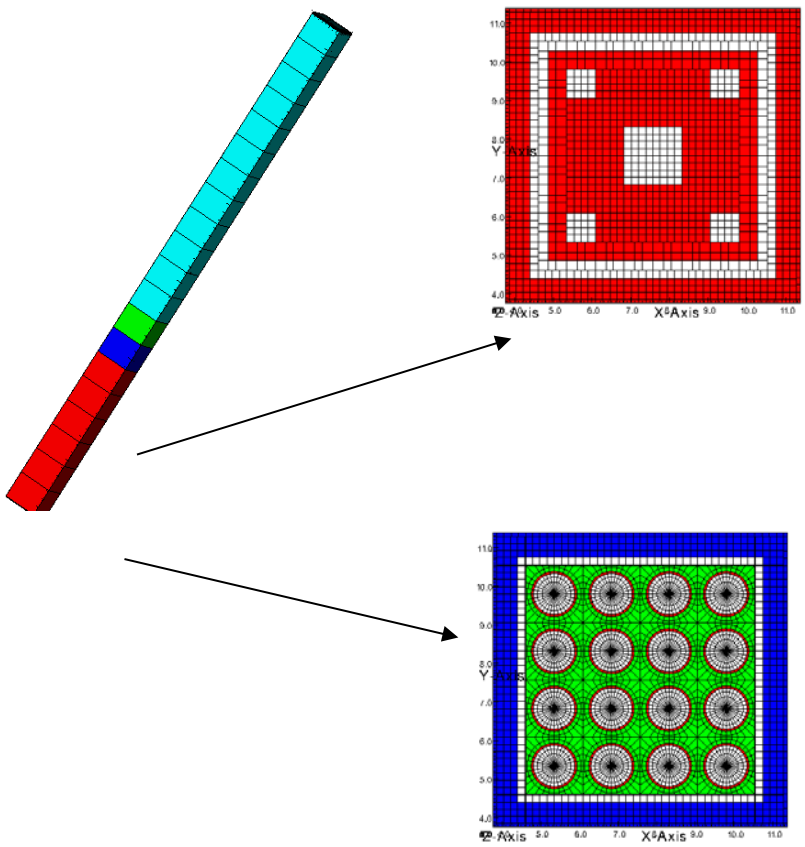

Figure 3-13: MPACT model for flux suppressors

The SPERT III E-core control rods and transient rod are inserted from different directions and the axial variation of the model composition is also shown in Figure 3-14. Note that this is just a generic depiction of the reactor; the control rod and transient rod heights do not correspond to any specific experiment.

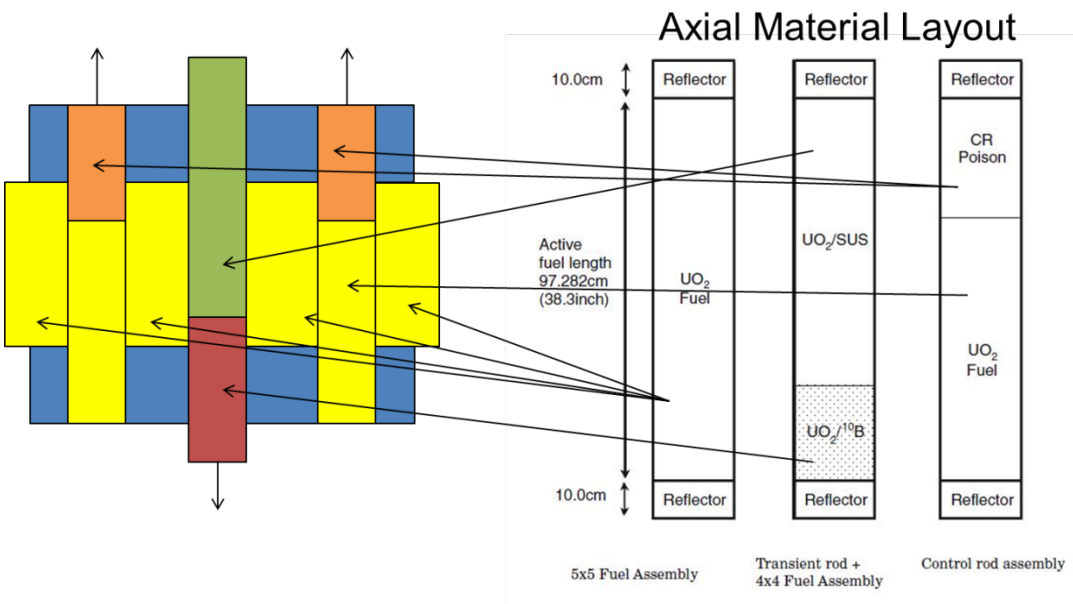

Figure 3-14: SPERT III E-core transient rod and control rod insertion

The MPACT model for the bottom of the active core is shown in Figure 3-15. In this section, the transient rod consists of the absorber region and the control rods consist of the fuel follower sections. The reactor vessel, thermal shield, and reactor core skirt are modeled with homogenous stainless steel with an inner diameter of 76.2 cm (32 inches).

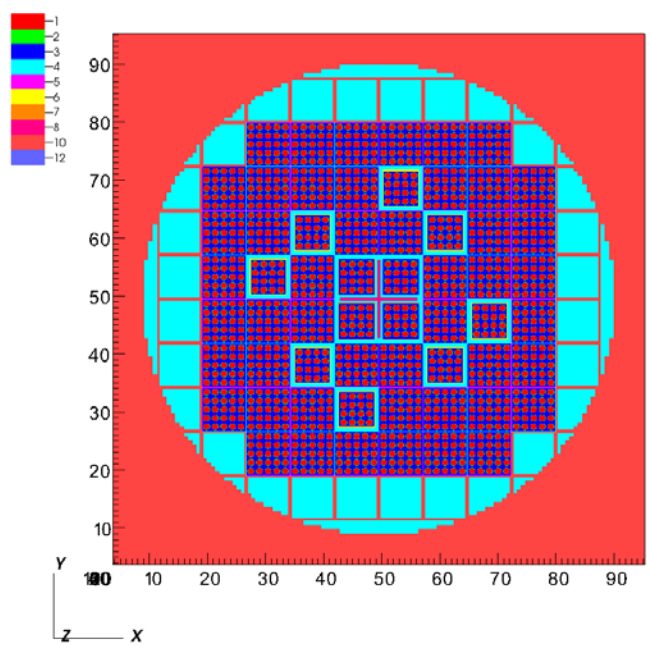

Figure 3-15: MPACT model for bottom of active core

The MPACT model for the flux suppressor region somewhere in the middle of the active core is shown in Figure 3-16. In this section, the transient rod consists of the non-absorber stainless steel section and the flux suppressors are clearly visible in the control rods. One of the two axial grids happens to be contained in the moderator as well.

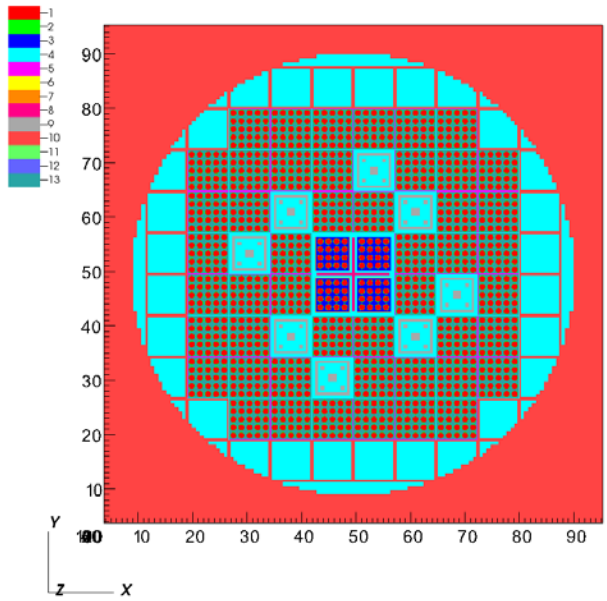

Figure 3-16: MPACT model for middle of active core

The MPACT model for the top of active core is shown in Figure 3-17. In this section, the transient rod consists of the non-absorber stainless steel section and the control rods consist of the absorber sections.

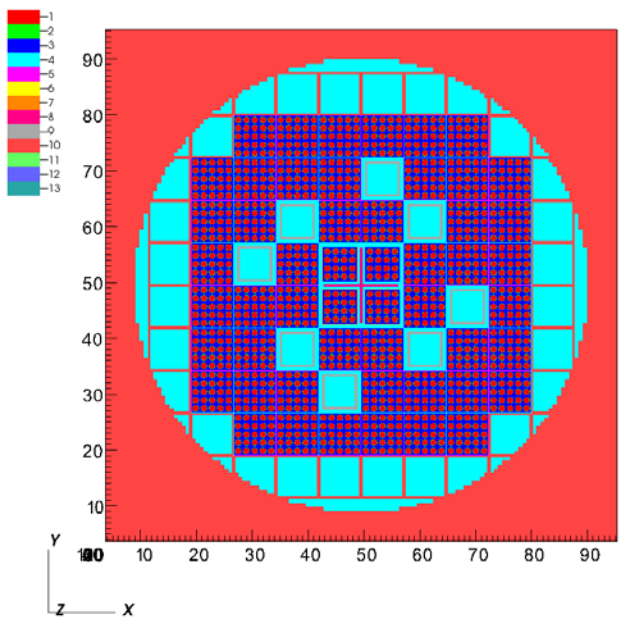

Figure 3-17: MPACT model for top of active core

The MPACT model for the bottom reflector is shown in Figure 3-18. In this section, the transient rod consists of the absorber region and the control rods consist of the fuel follower sections. The 16-rod transient assemblies and 25-rod assemblies are below the active fuel level and modeled as stainless steel end plugs in this section.

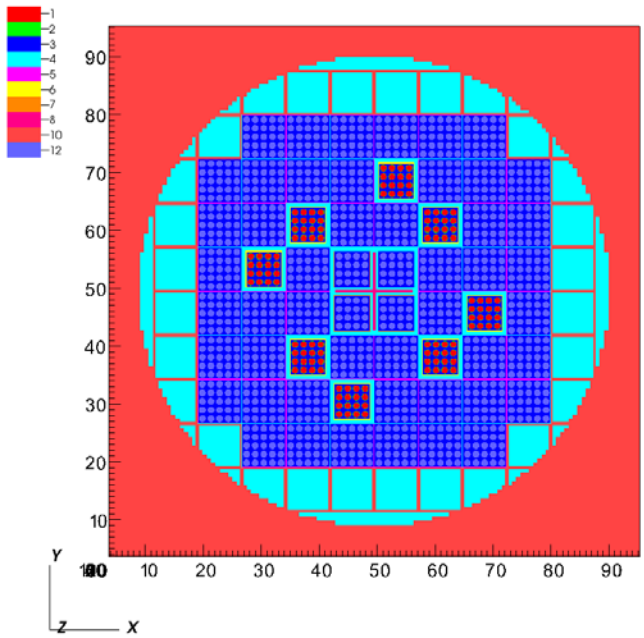

Figure 3-18: MPACT model for bottom reflector

The MPACT model for lower plane of the top reflector is shown in Figure 3-19. In this section, the transient rod consists of the non-absorber stainless steel section and the control rods consist of the absorber sections. The 16-rod transient assemblies and 25-rod assemblies are above the active fuel level and modeled as expansion space stainless steel compression springs occupying 5% of the space in this section.

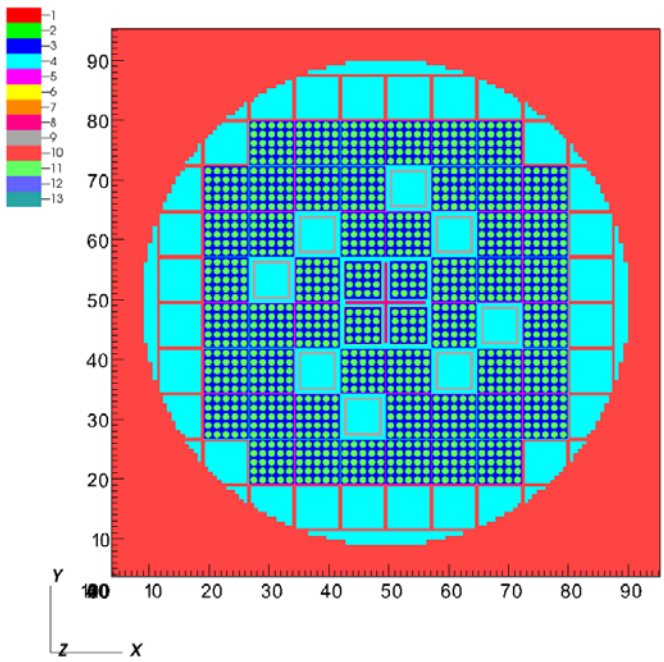

Figure 3-19: MPACT model for lower plane of top reflector

The MPACT model for the upper plane of top reflector is shown in Figure 3-20. In this section, the transient rod consists of the absorber region and the control rods consist of the absorber sections. The 16-rod transient assemblies and 25-rod assemblies are above the active fuel level and modeled as stainless steel end plugs in this section.

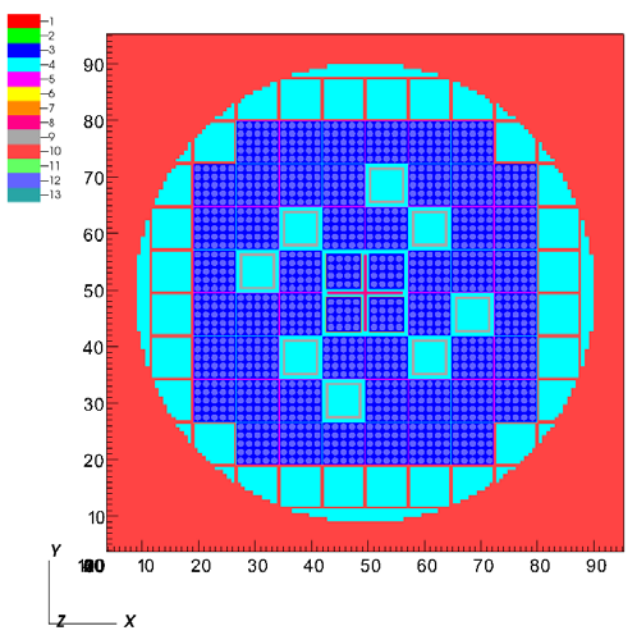

Figure 3-20: MPACT model for upper planes of top reflector

The thicknesses of axial meshes are selected to exactly model the critical control rod position. Generally, the whole model includes 2 axial meshes for the lower reflector, 2 axial meshes for the upper reflector, and 16 axial meshes for the active core. The specific thickness for each plane is determined by the control rod position. A typical thickness is around 6 cm.

3.3 KENO Model of SPERT

The SPERT III KENO model was developed to exactly mimic the geometry of the SPERT III MPACT model. Sub-meshing was not performed in KENO, however, since it is unnecessary for Monte Carlo type calculations. There are only two differences between the KENO and MPACT SPERT III models: 1) the reactor containment vessel is explicitly modeled as a cylinder in KENO, rather than approximated on a rectangular grid as in the MPACT model and 2) a small offset (1E-5 cm) is utilized in the KENO model to ensure that holes do not overlap. These minor discrepancies should have negligible effect on the results of the simulations. The SPERT III KENO simulations were run in continuous energy mode with 5,000 generations consisting of 5E6 neutrons per generation.

In order to calculate pin powers throughout the core, a separate unit for each region of interest must be created. KENO does offer mesh tally capabilities, but only the flux can be tallied, not reaction rates. KENO does not have the ability to explicitly calculate pin powers, so fission rates are calculated instead. While fission rates are not precisely proportional to pin power, they should be very close for a Light Water Reactor (LWR) such as SPERT III.

Figure 3-21 through Figure 3-26 are depictions of the KENO model taken at the same axial plane as Figure 3-15 through Figure 3-20. Additionally, Figure 3-27 shows a vertical slice through the core which provides an overview of the axial variation.

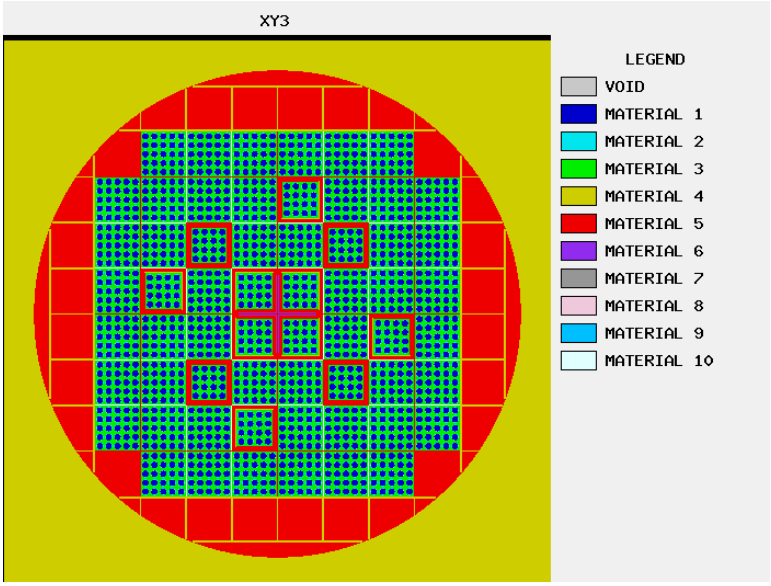

Figure 3-21: KENO model for bottom of active core

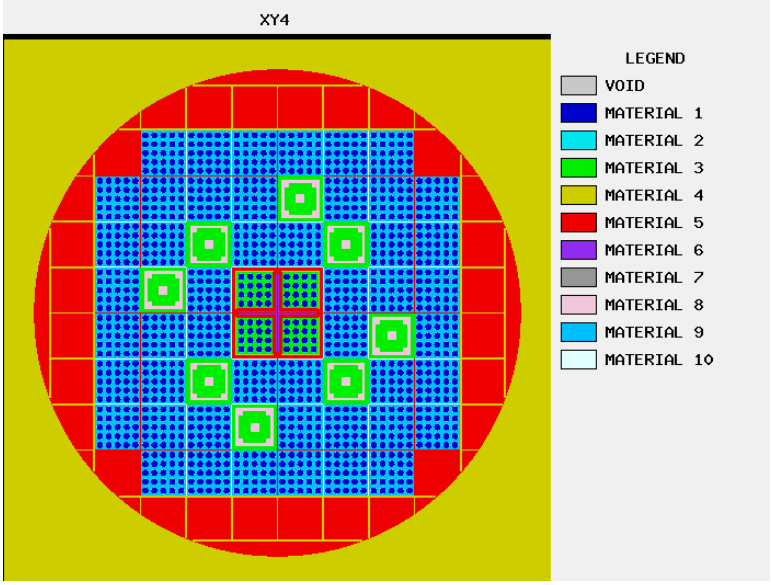

Figure 3-22: KENO model for middle of active core

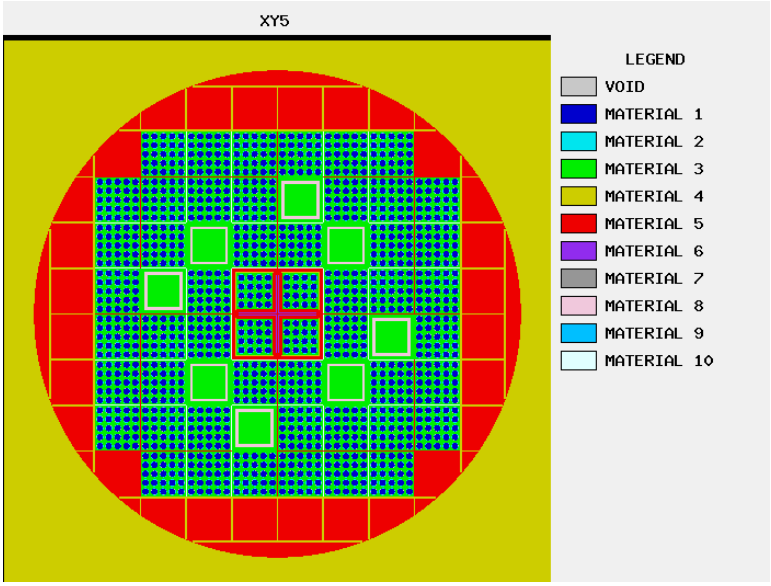

Figure 3-23: KENO model for top of active core

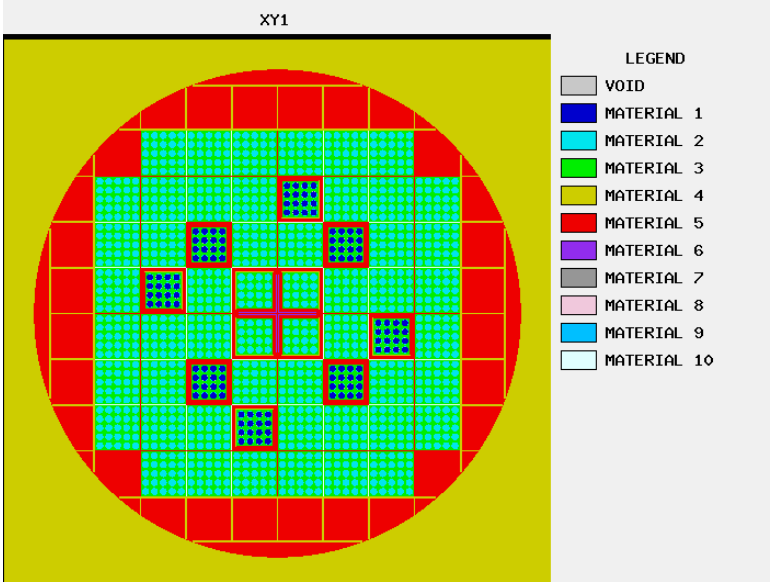

Figure 3-24: KENO model for bottom reflector

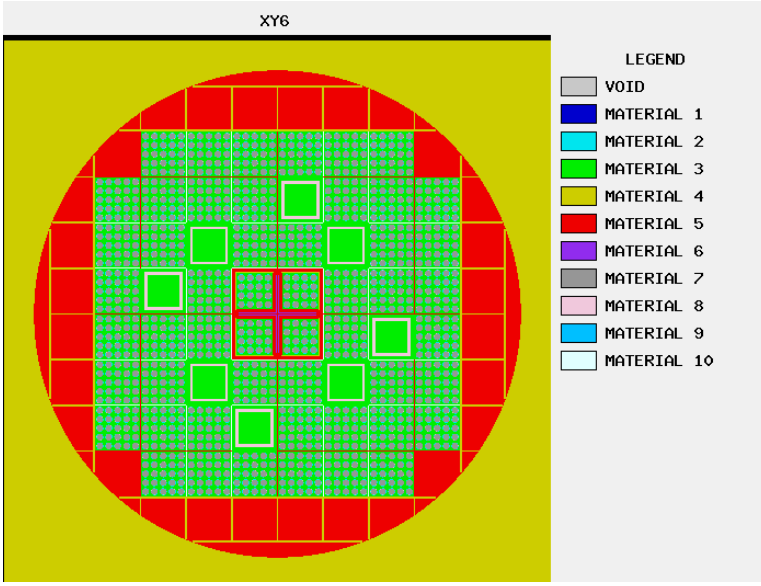

Figure 3-25: KENO model for lower plane of top reflector

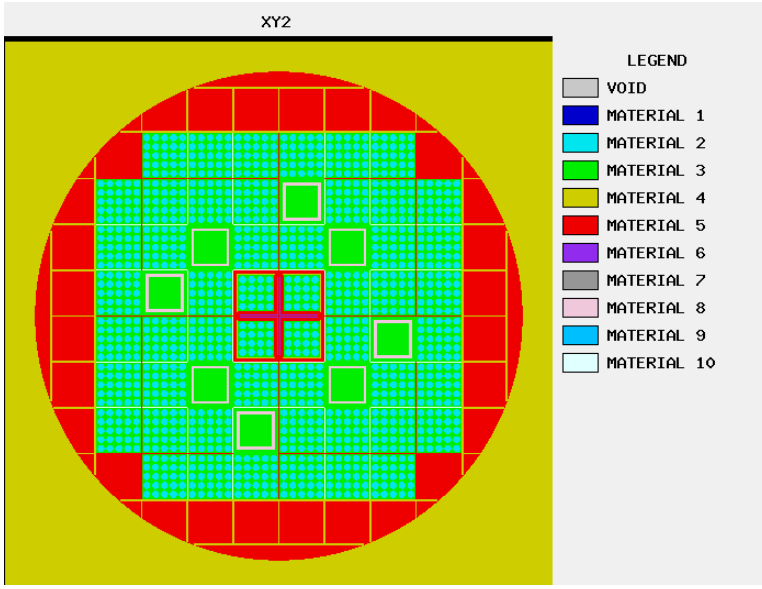

Figure 3-26: KENO model for upper planes of top reflector

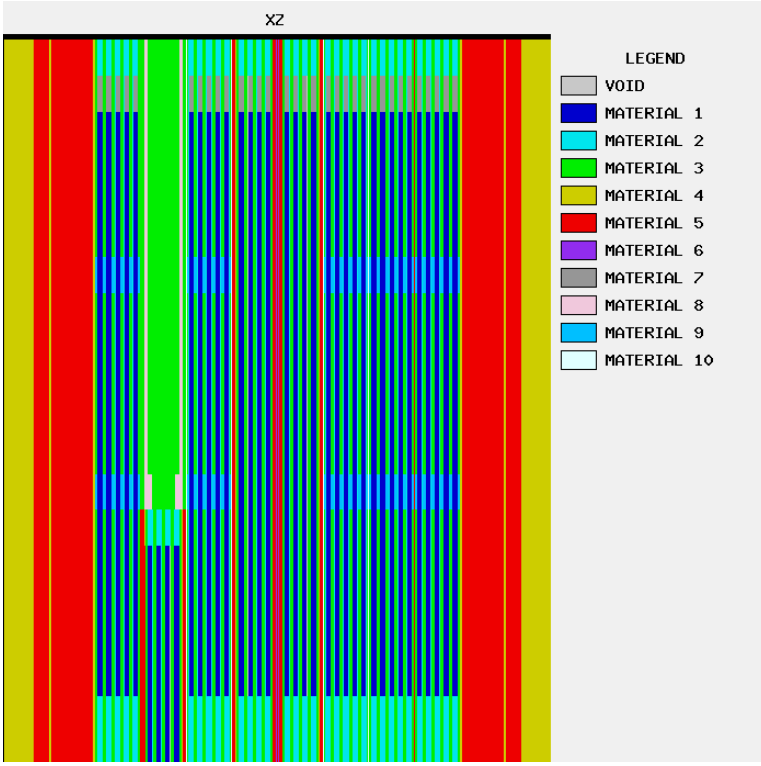

Figure 3-27: Vertical slice of the KENO model (CZP)

4.0 Results for SPERT Simulation

This section will review the results of SPERT simulation. The following section will first compare the Steady-state critical results for both KENO and MPACT to the experimental measurements. The MPACT transient results for two of the SPERT tests will then be presented in section 4.2.

4.1 Steady-State Critical Solutions for the SPERT III E-core with MPACT and KENO

The cold zero power (CZP) and hot zero power (HZP) critical cases of the SPERT III E-core were analyzed with MPACT using P2 scattering with 0.05 cm ray spacing, and the Chebyshev-Gauss quadrature set was used with 16 azimuthal and 4 polar angles. The multi-group NEM diffusion kernel was used to perform the axial solution, and both CZP and HZP cases were run with 20 axial planes using 720 cores. The fast and thermal fluxes computed by MPACT at the core mid-plane are shown in Figures 4-1 and 4-2 for the CZP and HZP cases, respectively . The location of the 5x5 and 4x4 rods in the core is very evident, as well as a distinct “fan blade” pattern in the fast flux.

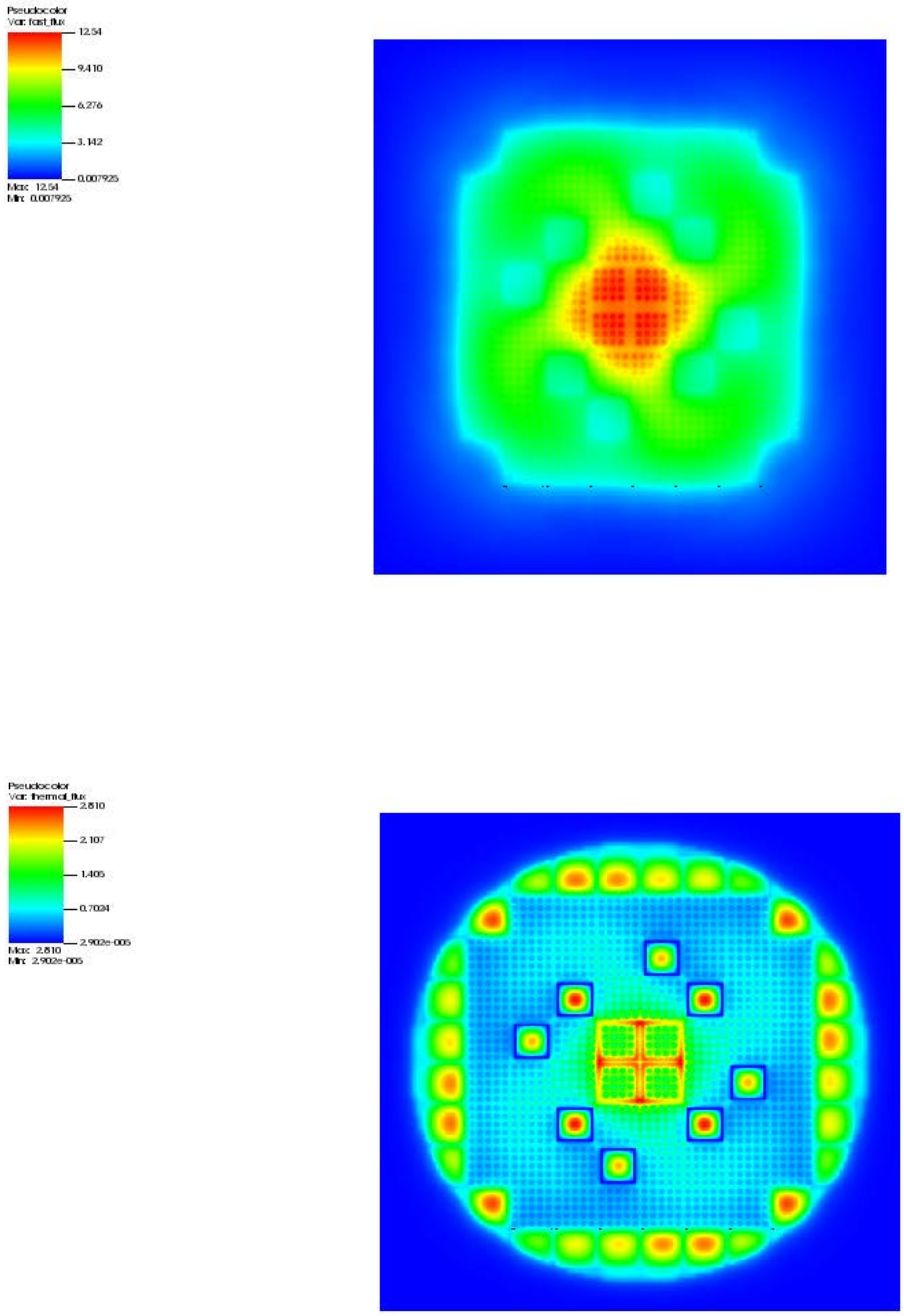

Figure 4-1 MPACT Fast (top) and Thermal (bottom) Flux for CZP

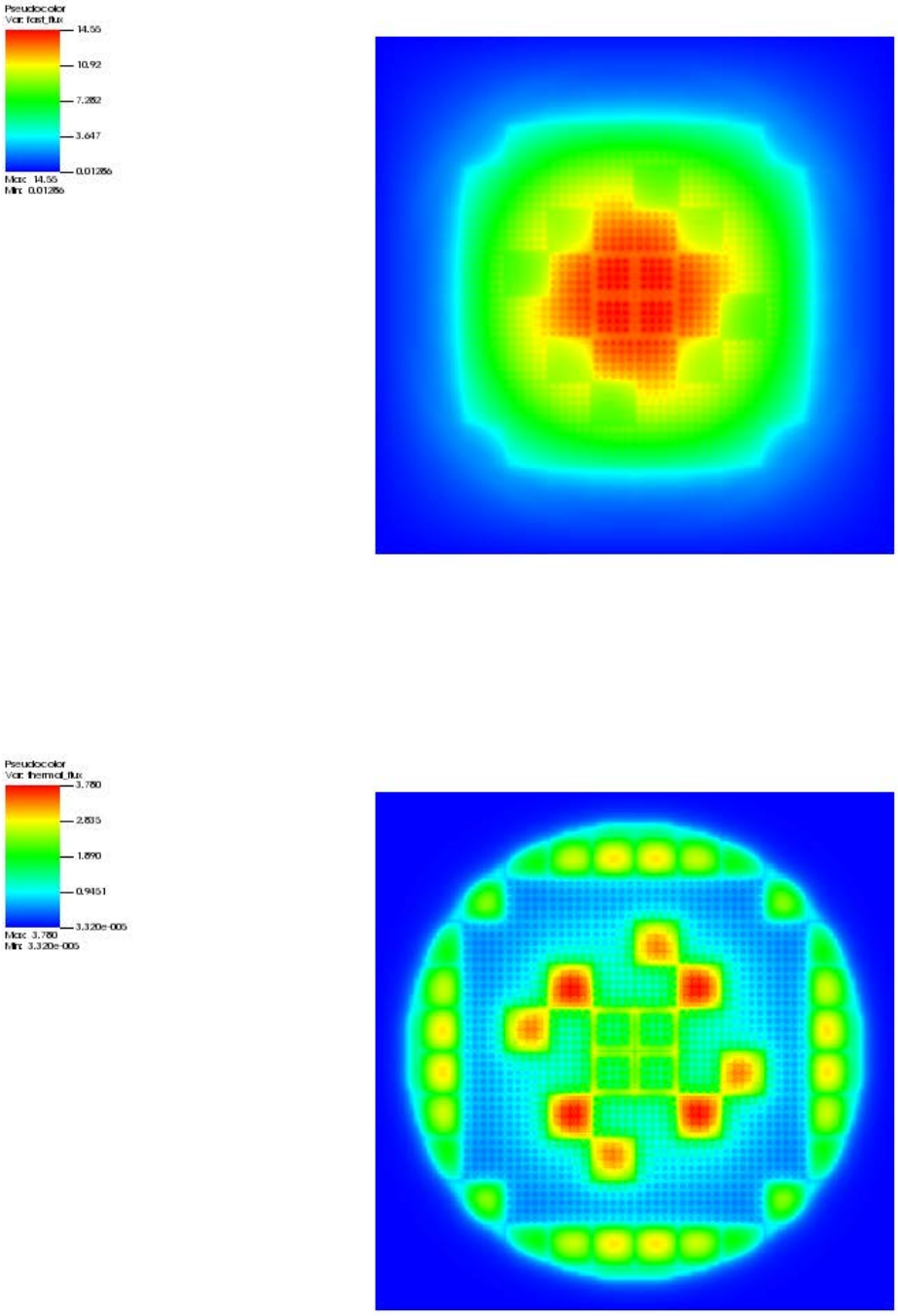

Figure 4-2 MPACT Fast (top) and Thermal (bottom) Flux for HZP

The eigenvalues computed by are compared with the eigenvalues computed by CE KENO for the CZP and HZP cases in Table 4-1. MPACT solutions were performed with both the ORNL 56 and 47 group libraries based on ENDF-VII. The critical control rod positions are also compared with S3K and PARCS Table 4.1

Table 4-1: Comparison of Eigenvalues

Case	Temp. (F)	C.R. Position(cm)	MPACT (56group)	MPACT (47group)	KENO-CE
CZP	70	36.957	0.99411	0.99613	1.00028 ±0.00001
HZP	550	71.755	0.99690	1.00023	1.00356 ±0.00001

Table 4-2: Comparison of Critical Control Rod Position

Case	Temperature (F)	Experiment	MPACT	S3K	PARCS
CZP	70	36.957	38.2	30.1	31.6
HZP	550	71.755	74.4	-	-

The axial power shapes calculated by KENO and MPACT are compared in Figure 4.3. As indicated there is good agreement for both CZP and HZP cases. The KENO radial power distribution at the peak plane (5) and and the top of the core plane (18) are shown in Figure 4.4 and 4.5, for the CZP and HZP cases, respectively.

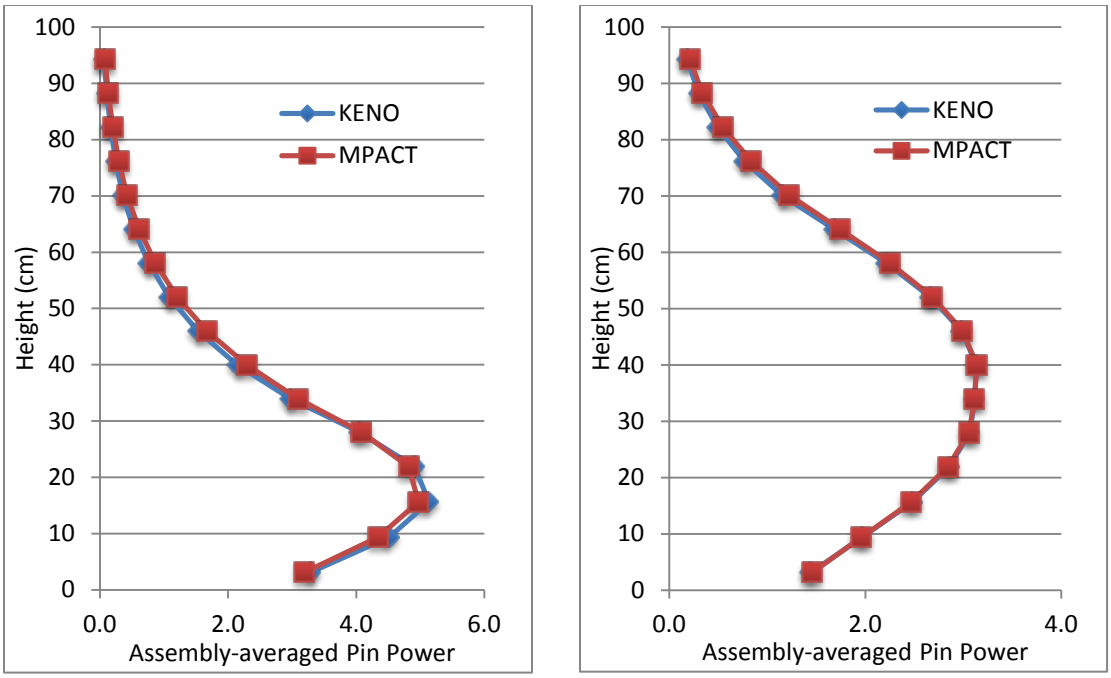

CZP **HZP**

Figure 4-3 Comparison of the CE KENO and MPACT Axial Power Shapes

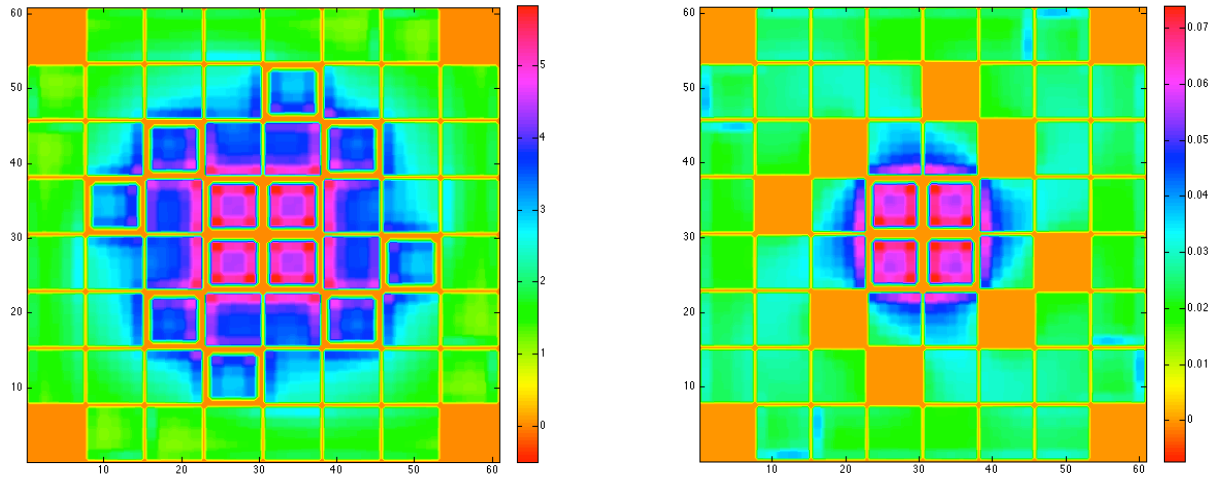

Figure 4-4 KENO CZP Radial Power Shapes at Peak Plane 5 (LHS) and Top of Core Plane 18 (RHS)

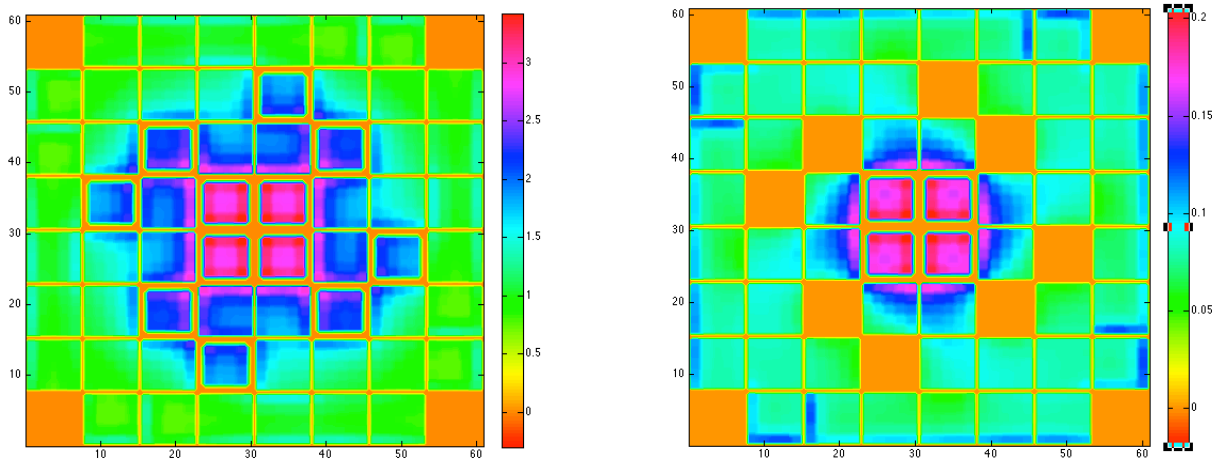

Figure 4-5 KENO HZP Radial Power Shapes at Peak Plane 8 (LHS) and Top of Core Plane 18 (RHS)

The fuel pin fission rate distributions calculated by KENO and MPACT are compared in Figures 4.6 and 4.7 for the peak fuel assembly in the CZP and HZP cores is located as shown below. As indicated the agreement between KENO and MPACT is very good, in particular for the HZP case.

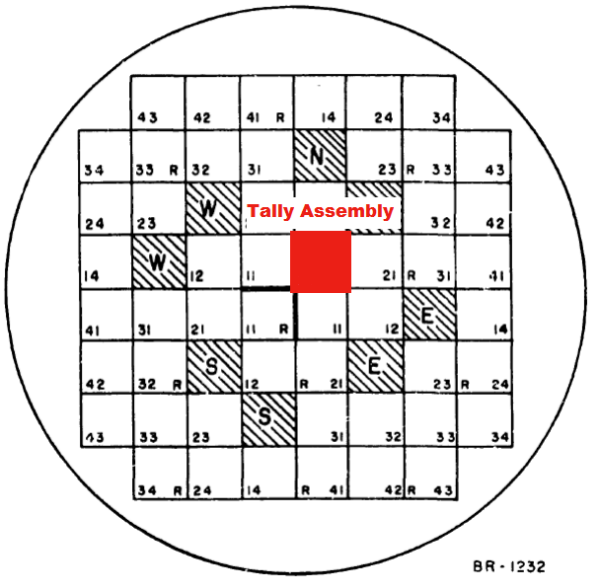

5.782 5.578 -3.53%	5.166 5.012 -2.98%	5.201 5.029 -3.31%	5.878 5.616 -4.45%
5.176 5.01 -3.21%	4.461 4.353 -2.41%	4.470 4.358 -2.49%	5.126 4.965 -3.14%
5.201 5.027 -3.35%	4.471 4.357 -2.54%	4.458 4.347 -2.48%	5.076 4.93 -2.87%
5.868 5.615 -4.30%	5.131 4.964 -3.25%	5.071 4.929 -2.80%	5.572 5.403 -3.03%

-------KENO
-------MPACT
-------Rel Dif

Figure 4-6 Comparison of Fission Rates Distribution (CZP)

3.248 3.244 −0.13%	3.048 3.050 0.08%	3.081 3.080 −0.02%	3.386 3.356 −0.90%
3.049 3.051 0.07%	2.816 2.826 0.36%	2.844 2.859 0.53%	3.169 3.166 −0.10%
3.085 3.082 −0.11%	2.847 2.860 0.44%	2.881 2.893 0.42%	3.189 3.195 0.20%
3.388 3.357 −0.91%	3.170 3.166 −0.13%	3.191 3.195 0.15%	3.451 3.447 −0.12%

Figure 4-7 Comparison of Fission Rates Distribution (HZP)

The very good agreement between MPACT and KENO for the steady-state critical cores provide confidence in the initial condition for the transient calculation.

4.2 Preliminary Transient Solutions for the SPERT III E-core with MPACT

The SPERT III E-Core control rod ejection tests consisted of a sequence of CZP, HZP, and HFP tests with various transient rod insertion depths. In the work performed here the HZP Test 60 and HFP Test 86 were chosen for preliminary validation of MPACT. The conditions for these test are shown in Table 4-3.

Table 4-3 SPERT III E-Core Experiments Modeled

Test	Initial Power (MW)	Pressure	Inlet Temp	TR Rod Worth ($)
60	-	1500 psi (10.3MPa)	500 F ± 4	1.23 ± 0.05
86	19 ± 1	1500 psi	502 F ± 4	1.17 ± 0.05

Transient test 60 is a hot-startup transient where the initial core temperature and core inlet temperatures are at 500 ^{o}F ± 4 ^{o}F. This temperature is achieved through direct heating on inlet coolant. The system is also pressurized such that the initial thermal hydraulic condition is within typical PWR operating conditions. In addition, the initial reactor power is approximately 50 W. However, because the data collection for this transient doesn't begin till approximately 0.17 seconds after the initiation of the transient, the actual initial core power was not provided in the documentation. It should also be noted that the position of the control rods prior to the transient are not indicated in the original documentation. In the model, the control rods are positioned such that k-effective values are maintained at approximate unity during the steady state. This ensures that the simulated transient begins with a true steady state reactor. The transient is initiated by accelerating the transient rod from its initial steady state inserted position to the bottom of the core. The acceleration is given as 2000 in./sec^2 or 50.8 m/sec^2. However, MPACT doesn't not currently allow control over the rate of movement of the ejected rod and a simplified scheme was used in which a series of composition changes was used to simulate the ramp of the control rod out of the core.

The SPERT cases for Tests 60 and 86 were run in MPACT using the 56 group ORNL library with P0 scattering, and a discretization with 0.05 ray spacing and the Chebyshev-Gauss quadrature set using 16 azimuthal and 4 polar angles. The transient fixed source problem was solved using the 2D-1D with the finite difference axial solver. A partial input for Test 60 is shown in Appendix B. As will be discussed in the future work section, the NEM transient kernel was developed and implemented in MPACT but preliminary calculations indicate that here are some numerical issues with the transient CMFD acceleration that remain to be resolved. Also, the results here were performed with an internal transient thermal-hydraulics (TH) and not with COBRA-TF which was not yet ready for transient coupling to MPACT. For these and other reasons noted in Section 5, the results here are considered preliminary and were not expected to provide consistent agreement with the experiments. Nonetheless, the transients calculations did converge and gave reasonable results within the limitations of the discretization and methods noted. The calculations were performed on 720 cores of the TITAN and each case required approximately 6 hours. Apartial listing of output is shown in Appendix C.

The preliminary transient results are shown in Table 4-4 for Test 60. The reactivity of the ejected rod was higher than the measured reactivity and the ejection time was quicker than the measured time. As shown in Figure 4-8, the pulse height was slightly higher and shifted to the left of the measured power. For Test 86, two cases were performed with different transient rod insertion depths. The first calculation used an initial transient rod position to provide a reactivity insertion consistent with the measured 1.17$ reactivity. In the second case, the rod insertion depth was adjusted to increase the reactivity insertion to provide a peak power closer to the measured power. The power versus time plot for each case is shown in Figure 4-9.

Table 4-4 Preliminary MPACT Results for SPERT III E-Core Tests 60/86

	Cases	Initial Power	Measured Reactivity($)	Rod Ejection Time (s)	Peak Power (MW)	Time to peak power
Test 60	Experiment	-	1.23 ± 0.05	0.10	415.1	0.216
	Calculation	~2kW	1.41	0.08	428.3	0.190
Test 86	Experiment	19 ± 1MW	1.17 ± 0.05	0.078	598.1	0.121

	Calculation 1	19MW	1.17	0.075	423.8	0.110
	Calculation 3	19MW	1.21	0.085	643.0	0.118

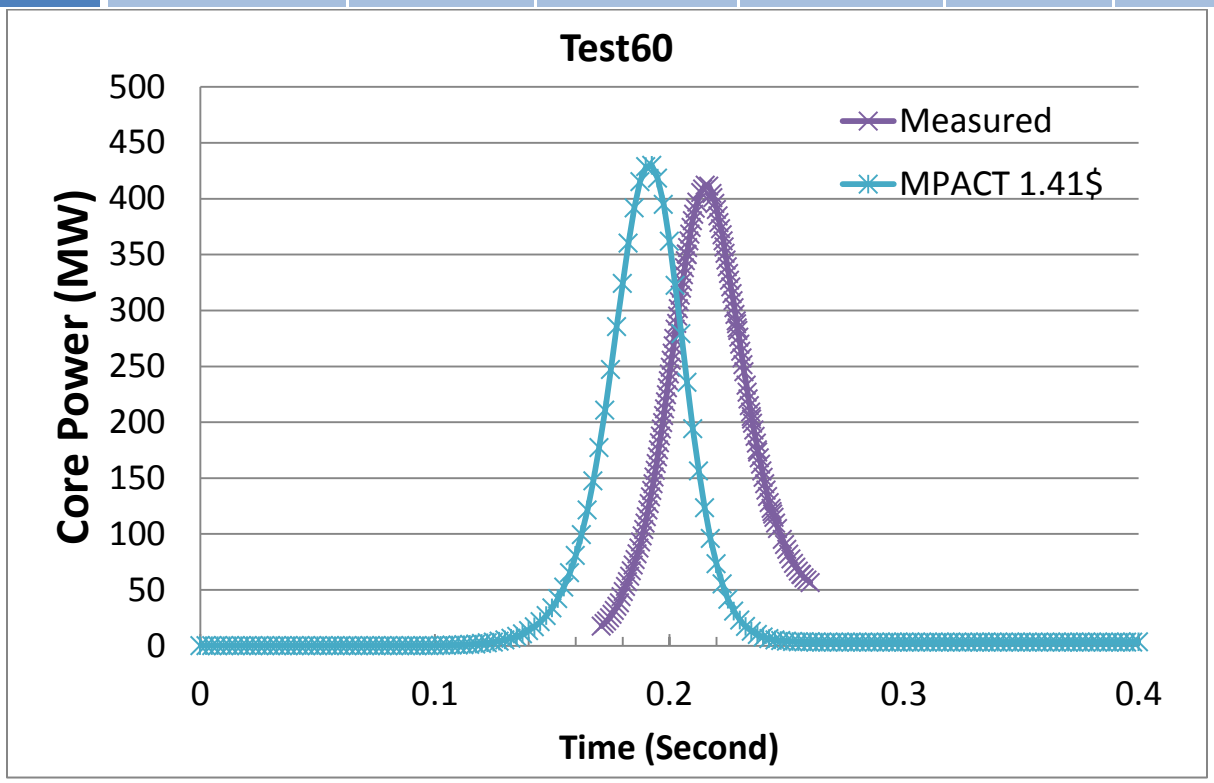

Figure 4-8 Preliminary MPACT Results for SPERT III E-Core Test 60

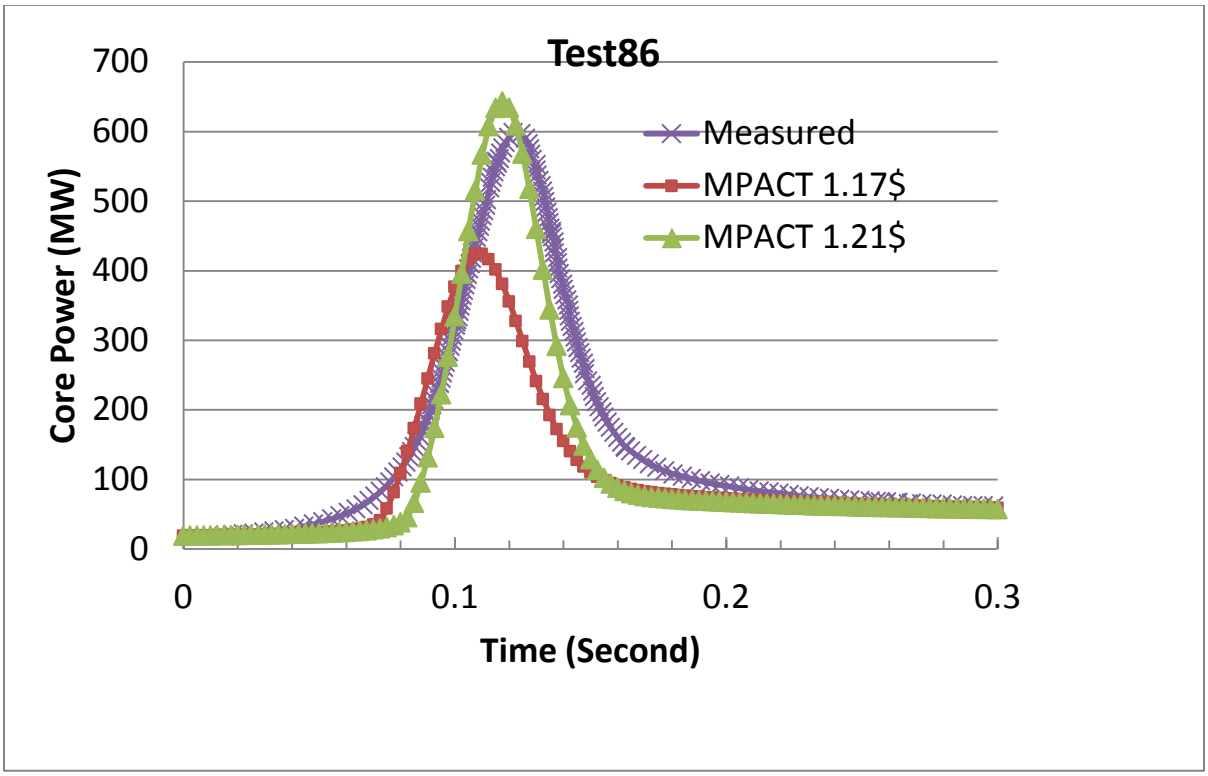

Figure 4-9 Preliminary MPACT Results for SPERT III E-Core Test 86

5. Summary / Continuing Work

5.1. Summary

This report summarized the second phase in the development, implementation, testing, and validation of the software modules in the MPACT neutron transport component required for a demonstrable transient capability necessary to support accident (e.g. RIA) scenarios. This work was a continuation of the first phase of the implementation which was reported in L3.RTM.SUP.P8.02 on March 31, 2014.

Section 2 of this report reviewed the transient methods implemented in MPACT which were modified slightly from those described in the March 31 report. Section 3 then described the modeling of the SPERT III E-Core using MPACT and KENO-CE. In section 4, the results of the MPACT steady-state modeling of SPERT III E-Core for the Cold Zero Power (CZP) and Hot Zero Power (HZP) critical experiments were compared were compared to the measured data and to the KENO-CE results. The steady-state validation of MPACT provided confidence in the initial condition for the transient simulations. Preliminary results for the a HZP and HFP transient were also shown in section 4. Some transient methods development work remains to be done, and therefore the transient results were not in as good agreement with the measured data as the steady-state. The work required to complete the transient methods and implementation will be discussed below.

5.2 Continuing Work

This section will summarize the areas requiring continuing work in order to complete the development and implementation of the transient capability in MPACT.

Library Development

MPACT is currently using a 56 group ORNL library which has since been replaced by a new 47 group library for production calculations. The kinetics parameters in the 56 group library were hand processed for the SPERT transient calculation. A full kinetics library should be processed for the new 47 group library.

Transient Physics Methods

Transient NEM with CMFD

As noted above, the transient calculation was performed with a finite difference kernel for the transient 2d-1d solution. Work was begun on a transient NEM kernel with CMFD as described in section 2. However, this work needs to be completed and tested within MPACT. The was a substantial difference in the eigenvalues and rod worths of the 2d-1d solution calculated with the finite difference and NEM 1d kernels. Also, some numerical issues were encountered with the initial implementation of the transient CMFD for NEM that need to be resolved in order to keep the computational times tractable.

NEM SP3 Transient

The base steady-state 1D kernel used in MPACT for LWRs is the SP3 method. In order to provide consistency between the steady-state and transient solvers, a NEM SP3 kernel would need to be developed and implemented in MPACT.

Code Mechanics

Some minor code modifications are necessary in order to provide a production quality code for RIA analysis. This would include a robust method for moving the control rod in the code that would provide flexibility for the user to match the measured rod ejection time.

Code Input / Output

XML Input

The current transient MPACT input for SPERT was provided in a native input. Modifications would be required in order for the input to be consistent with the XML input currently used for steady-state LWR analysis in VERA-CS.

Reactivity Edits

Reactivity edits are a standard output used for LWR RIA analysis and should be implemented in MPACT along with the standard visualization tools used for code transient LWR analysis. The reactivity edits would require the implementation of the steady-state adjoint flux in MPACT.

6. References

[Durgone, 1965] J. Durgone, *SPERT III Reactor Facility: E-CORE Revision*, AEC Research and Development Report IDO-17036, November 1965.

[Aoki, 2009] S. Aoki, T. Suemura, J. Ogawa, T. Takeda, "Analysis of the SPERT-III E-Core Using ANCK Code with Chord Weighting Method," *Journal of Nuclear Science and Technology,* **Vol. 6,** p. 243 (2009).

[McCardell, 1969] R.K. McCardell, D.I. Herborn, J.E. Houghtaling, *Reactivity Accident Test Results And Analysis for the SPERT III E-Core – A Small Oxide-Fueled, Pressurized-Water Reactor*, AEC Research and Development Report IDO-17281, March 1969.

[Wang, 2013] R. Wang, T. Downar, Y. Xu, N. Hudson, "Validation of the U.S. NRC Coupled Code System TRITON/TRACE/PARCS using the Special Power Excursion Reactor Test III," *Nuclear Technology,* Vol. 183, Sep. 2013.

[Bowman, 2011] S. M. Bowman, "SCALE 6: Comprehensive Nuclear Safety Analysis Code System," *Nucl. Technol*. **174**(2), 126-148, May 2011.

[Grandi, 2013] G. Grandi and L. Moberg, "Qualification of CASMO5/SIMULATE-3K Against the SPERT III E-Core Cold Start-up Experiments," PHYSOR-2012, Knoxville, TN, 2012.

Appendix A

REACTOR COMPONENT DESIGN DATA

[Ref. 1, Page 99, Ref. 2, Page 85]

Core: (Operational Loading)
- Configuration -- cylinder (approximately)
- Diameter -- ~ 30 inches
- Active height -- 38.3 inc~es
- Volume -- 2.21 x 104 in.
- Composition:
  - Water -- 6.7 weight percent
  - Stainless steel -- 22.5 weight percent
  - UO_2 -- 70.8 weight percent
  - U -- 62.4 weight percent
  - U-235 -- 3.0 weight percent
- Fuel load, U-235 -- 57.4 Kg (53.6 Kg)
- Number of fuel assemblies, all types – 64 (60)

Fuel. Elements:
- Type -- rectangular, rod type
- Number (Operational Loading)
  - 25-rodassembly – 52 (48)
  - 16-rodassembly-- 4
  - Control rod assembly -- 8
- Overall Dimensions:
  - 25-rod assembly -- 2.975 by 2.975 by 52.750 inches
  - 16-rod assembly -- 2.476 by 2.476 by 52.750 inches
  - Control rod fuel section -- 2.496 by 2.496 by 45-41/64 inches
- Fuel content:
  - 25-rod assembly -- 962.5 g U-235
  - 16-rod assembly -- 616 g U-235
  - Control rod assembly -- 616 g U-235
- Pitch -- 0.585 inches (square)
- Flow area (inside)/element:. 2
  - 25-rod assembly -- 4.29 $in.^2$
  - 16-rod assembly -- 3.16 $in.^2$
  - Control rod assembly -- 2.80 $in.^2$
- Heat transfer area (active fuel length)

25-rod assembly -- 1402 in.^{2}
16-rod assembly -- 897 in.^{2}
Control rod assembly -- 897 in.^{2}

Fuel Rods:
- Type -- cylindrical
- Materials:
  - Fuel tube -- stainless steel, Type 348
  - Pellets -- 4.8 percent enriched sintered UO_2 (10.5 g/cm^3)
- Fuel pellet dimensions:
  - Long pellet-- 0.420 inches OD by 0.766 inches
  - Short pellet -- 0.420 inches OD by 0.511 inches
- Rod dimensions:
  - Diameter -- 0.466 inches OD
  - Wall thickness -- 0.020 inches
  - Overall length -- 40.8 inches (excluding end plugs)
  - Active length -- 38.3 inches
- U-235/rod -- 38.5 g
- Gas gap -- 0.003 inches helium

Control Rods:
- Type -- rectangular; upper-section is absorber material, lower section is a fuel subassembly
- Number -- 8
- Composition:
  - Absorber section -- 1.35-weight-percent boron-10 in Type 18-8 stainless steel; 0.186-inch-thick hollow square box
  - Fuel section -- see fuel assembly section above
- Overall dimensions:
  - Absorber section (nom) -- 2.496 by 2.496 by 45-31/32 inches
  - Fuel section (nom) -- 2.496 by 2.496 by 45-41/64 inches
- Travel -- 45 inches maximum
- Average scram time -- 0.350 sec
- Withdrawal Rates:
  - Fast speed -- 17.4 in./min
  - Medium speed -- 11.5 in./min
  - Slow speed -- 5.6 in./min

Transient Rod:
- Type -- cruciform; lower section, absorber material; upper section, 18-8stainless steel
- Number -- 1
- Composition -- 1.35 weight percent boron-10 in 18-8 stainless steel
- Dimensions:
  - Thickness of blades -- 3/16 inches
  - Blade width -- 5-1/8 inches
  - Absorber-section length -- 38 inches
- Travel -- 45 inches max
- Average drop time -- 0.2 sec

React - Vessel
- Construction
  - Shell -- layer type

Top head -- forged, full-opening, flanged, hemispherical
Bottom head -- layer type
Inside diameter -- 48 in.
Shell thickness (including clad) -- 3.25 in.
Head thickness -- 3.5 in.
Materials
Outer shell plate -- carbon steel plates 1/4 in. thick
Inner shell plate -- magnesium-vandium steel (ASTM A225 GrB) with a 1/8-in.-thick 304L stainless steel clad
Top head -- carbon steel manually clad with Type 309 stainless steel
Design pressure
Working pressure -- 2500 psig
Estimated maximum transient pressure -- 3500 psig
Design temperature -- 700OF
Overall length (includes head) -- 19 **ft** 11-1/8 in.
Maximum diameter of head flange -- 5 **ft** 7 in.
Number of thermal shields -- 5 (including reactor flow skirt)
Total thickness of shields -- 5.75 in.
Average length of shields -- 45.5 in.
Inside diameter of inner shield -- 32 in.
Weight of vessel
Shell 55,784 lb
Head 10,606 lb
Bottom tee 5,580 lb
Shield 11,430 **lb**
Total 83,400 **lb**
Insulatlon -- 4 in. of foamglass

Appendix B

MPACT Partial Input for SPERT Test 60

```
CASEID spert_60_tr24
STATE
  rated_power  20.0
  rated_flow   14.0 fps
  tinlet       260.0
  core_power   0.2  ! 40 kW

XSEC
  xslib ORNL declib56g_e7_09042013_p0mixed.fmt

! Flow area is 7.62^2 - npins*pinArea, then multiplied by nAssem
! This will get an approximate flow rate for the fuel assemblies correct
! It will be wrong for non-fuel assemblies, but that won't be a game
! changer for now
! I then multiplied the flow area by the water density and flow speed
! to get an approximate mass flow rate
MATERIAL
! The fuel is in the form of uranium dioxide pellets,
! 4.8 weight percent enriched, 0.420 inch in diameter.
! Each of the fuel rods contain 38.5 grams of U-235
! with an active fuel length of 38.3 inches
  mat  1 2 UO2  500 F 10.5 g/cc   \   8016 4.68572E-02
                                     92235 1.13826E-03
                                     92238 2.22903E-02
! SS 348 + (12.4546 0as gap)
! The materials of the tubingand end plugs
! are Types 348 and 347 stainless steel, respectively
  mat  2 0 CLAD  500 F 7.0299 g/cc \  6000 1.40991E-04
  mat  2 0 CLAD  500 F 7.0299 g/cc \  6000 1.40991E-04

! Coolant inside box which may be heated
  mat  3 1 Coo 500 F 0.79568    g/cc \   1001 5.33165E-02
  mat  3 1 Coo 500 F 0.79568    g/cc \   1001 5.33165E-02
                                        8016 2.66582E-02
                                        ! moderate out of box
  mat  4 1 Mod 500 F 0.79568    g/cc \  1001 5.33165E-02
  mat  4 1 Mod 500 F 0.79568    g/cc \  1001 5.33165E-02
                                       8016 2.66582E-02
```

```
! BOX for 5x5: SS(type not determined) + 25% water for the slots
!  if smear with water gap, then there are 50% water
! A total area of 120 square inches in the form of slots
! has been removed from each stainless steel fuel can

(note:   mat cards deleted )

!
GEOM
GEOM
 file ./geom_60_tr24.inp


 core 360
   8  8  8  8 32 31 29 30  8  8  8  8
   8  8 35 34  7  7  7  7 27 28  8  8
   8 37 36  1  1  1  1  1  1 24 25  8
   8 38  1  1  1  1  2  1  1  1 23  8
  40  7  1  1  2  1  1  2  1  1  7 22
  41  7  1  2  1  4  3  1  1  1  7 20
  42  7  1  1  1  5  6  1  2  1  7 19
  43  7  1  1  2  1  1  2  1  1  7 18
   8 45  1  1  1  2  1  1  1  1 16  8
   8 46 47  1  1  1  1  1  1 14 15  8
   8  8 48 49  7  7  7  7 12 13  8  8
   8  8  8  8 51 52  9 10  8  8  8  8

OPTION
  bound_cond 0 0 0 0 0 0
  solver 1 2
!  nodal T NEM-MG
  nodal F
  ray 0.05 CHEBYSHEV-GAUSS 4 1
  parallel 720 1 1 2
  cmfd T MGNODE
  scatt_meth P0
  param 2D1D->splitTL SBK .TRUE.
  param 2D1D->TLtreatment STRING FLAT
  internalth T SS
  vis_edits F F
  validation F

TRANS
  enable T
  time 0.6 / 0.0025
  method theta 0.5
  perturb 0.0    0.1   RAMP  1 / 14  14 8
  perturb 0.1    0.6   CONST 1 /  8  8  8

XS Library File Name     = declib56g_e7_09042013_
```

Appendix C

MPACT Iteration History for SPERT Test 60

```
000:00.01 Processing Input...
  000:00.01 Scanning input...
  000:00.01   Scanned Block CASEID
  000:00.01   Scanned Block STATE
  000:00.01   Scanned Block XSEC
  000:00.03   Scanned Block MATERIAL
  000:00.28   Scanned Block GEOM
  000:00.28   Scanned Block OPTION
  000:00.29   Finished reading Block STATE
  000:00.29   Finished reading Block XSEC
  000:00.36   Finished reading Block MATERIAL
  002:58.42   Finished reading Block GEOM
  002:58.44   Finished reading Block OPTION
  002:58.46   Finished reading Block TRANS
  002:58.50 Processing XS Libraries...
  003:00.09 Generating Materials...
  003:00.19 Generating Reactor Geometry...
  003:00.20 Generating Reactor Mesh...
  003:42.63 Initializing Parallel Environment...
  003:43.50 Setting up angular quadrature...
  003:43.55 Initializing mesh...
  003:43.96 Generating Input Edits...
                Setting up modular rays...
                Performing ray tracing...
  003:44.54 Initializing Base MOC Sweeper...
                Setting up long rays...
  003:44.54 MOC Sweeper initialization complete
  003:44.54 Initializing PS 2D1D Sweeper...
                      ...with TL splitting
                      ...with LFLAT TL spatial treatment
                      ...with ISO TL angular treatment
  003:44.59 Initializing Multi-group Fixed Source Solver...
                Default convergence norm is being used
                Default step algorithm is being used
                Default solve algorithm is being used
  003:45.24 Initializing Eigenvalue Solver...
                Adding eigenvalue accelerator...
                 -CMFD acceleration is being used (MG LS, Node-Major)
                      ...with P0 boundary update
                      ...not using angle decomp processors
```

```
003:46.19 Initializing Internal TH Solver...
003:46.20 Initializing Feedback Solver...
003:46.51 Initializing MultiState Solver...
003:46.58 Initializing Transient Solver...
003:48.15 Computing Internal TH...
003:48.49       Outlet temperature was 5.342384E+02 K...
003:48.49       Maximum fuel temperature was 5.348174E+02 K...
003:48.49       Maximum temperature change was 1.643376E+00 K...
003:48.49       Average fuel temperature was 5.346576E+02 K...
003:48.49       Maximum moderator density change was 1.452874E-01 g/cc...
003:49.78 Using P0 in All Regions...
003:49.78 Performing Eigenvalue Calculation...
003:49.78      iter    keff     norm_keff    norm_fissrc
003:49.78         0  1.0000000 1.000000E-05 1.000000E-04
          MG-CMFD   10  0.9376926 2.090190E+00
          MG-CMFD   20  0.9381203 2.107335E-01
          MG-CMFD   30  0.9381077 2.228607E-02
          MG-CMFD   40  0.9381065 2.365995E-03
          MG-CMFD   45   262    0.9381064   7.709317E-04
          1G-INNER   2        228           1.438965E-01
008:55.82 Computing Internal TH...
008:56.08       Outlet temperature was 5.342395E+02 K...
008:56.08       Maximum fuel temperature was 5.358474E+02 K...
008:56.08       Maximum temperature change was 9.982828E-01 K...
008:56.08       Average fuel temperature was 5.346755E+02 K...
008:56.08       Maximum moderator density change was 2.105435E-05 g/cc...
008:56.09 Calculating Equivalence XS...
          Solving Subgroup FSP...
          Group  16 Cat  2 92235    16 6.2978E-07
          Group  16 Cat  1 92238    16 6.2978E-07
          Group  17 Cat  2 92235    16 7.6044E-07
          Group  17 Cat  1 92238    16 7.6044E-07
          Group  18 Cat  2 92235    16 6.5814E-07
          Group  18 Cat  1 92238    16 6.5814E-07
          Group  19 Cat  2 92235    16 9.7202E-07
          Group  19 Cat  1 92238    16 9.7202E-07
          Group  20 Cat  2 92235    16 6.2978E-07
          Group  20 Cat  1 92238    16 6.2978E-07
          Group  21 Cat  2 92235    16 8.5688E-07
          Group  21 Cat  1 92238    16 8.5688E-07
          Group  22 Cat  2 92235    16 6.2978E-07
          Group  22 Cat  1 92238    16 6.2978E-07
          Group  23 Cat  2 92235    16 6.3418E-07
          Group  23 Cat  1 92238    16 6.3418E-07
          Group  24 Cat  2 92235    20 6.6917E-10
          Group  24 Cat  1 92238    20 6.6918E-10
          Group  25 Cat  2 92235    16 8.7118E-07
          Group  25 Cat  1 92238    16 8.7118E-07
          Group  26 Cat  2 92235    16 9.8351E-07
          Group  26 Cat  1 92238    16 9.8351E-07
          Group  27 Cat  2 92235    20 2.6513E-08
          Group  27 Cat  1 92238    20 2.6513E-08
          Group  28 Cat  2 92235    16 6.2978E-07
```

```
          Group  28 Cat  1 92238    16 6.2978E-07
          Group  29 Cat  2 92235    16 6.2978E-07
          Group  29 Cat  1 92238    16 6.2978E-07
          Group  30 Cat  2 92235    20 6.4310E-09
          Group  30 Cat  1 92238    20 6.4310E-09
          Group  31 Cat  2 92235    16 6.2978E-07
          Group  31 Cat  1 92238    16 6.2978E-07
          Group  32 Cat  2 92235    16 6.5474E-07
          Group  32 Cat  1 92238    16 6.5474E-07
          Group  33 Cat  2 92235    20 4.3886E-08
          Group  33 Cat  1 92238    20 4.3886E-08
          Group  34 Cat  2 92235    20 6.9230E-07
          Group  34 Cat  1 92238    20 6.9230E-07
          Group  35 Cat  2 92235    20 1.5370E-08
          Group  35 Cat  1 92238    20 1.5370E-08
          Group  36 Cat  2 92235    16 6.2978E-07
          Group  36 Cat  1 92238    16 6.2978E-07
          Group  37 Cat  2 92235    16 6.8387E-07
          Group  37 Cat  1 92238    16 6.8387E-07
          Group  38 Cat  2 92235    16 6.2978E-07
          Group  38 Cat  1 92238    16 6.2978E-07
          Group  39 Cat  2 92235    16 6.2978E-07
          Group  39 Cat  1 92238    16 6.2978E-07
          Group  40 Cat  2 92235    16 6.3269E-07
          Group  40 Cat  1 92238    16 6.3269E-07


                              ……

010:32:42 Using P0 in All Regions...
010:32:42 @t= 5.97500E-01 p= 9.30871E+01   5
010:32:52 Solving transient t= 6.000E-01...
010:32:53 Using P0 in All Regions...
          1G-INNER   2        228           1.814698E-02
          TRANSIENT    1   1.023913E-01   1.814698E-02
          1G-INNER   2        228           1.503611E-03
          TRANSIENT    2   8.504450E-03   1.503611E-03
          1G-INNER   2        228           1.579076E-04
          TRANSIENT    3   8.921866E-04   1.579076E-04
          1G-INNER   2        228           2.313804E-05
          TRANSIENT    4   1.305871E-04   2.313804E-05
          1G-INNER   2        228           3.471764E-06
          TRANSIENT    5   1.951931E-05   3.471764E-06
010:34:38 Computing Internal TH...
010:34:38       Outlet temperature was 5.342403E+02 K...
010:34:38       Maximum fuel temperature was 7.967734E+02 K...
010:34:38       Maximum temperature change was 1.734108E-01 K...
010:34:38       Average fuel temperature was 5.874706E+02 K...
010:34:38       Maximum moderator density change was 3.573176E-10 g/cc...
010:34:38 Calculating Equivalence XS...
          Solving Subgroup FSP...
          Group  16 Cat  2 92235    16 6.2978E-07
          Group  16 Cat  1 92238    16 6.2978E-07
```

```
          Group  17 Cat  2 92235    16 7.6044E-07
          Group  17 Cat  1 92238    16 7.6044E-07
          Group  18 Cat  2 92235    16 6.5814E-07
          Group  18 Cat  1 92238    16 6.5814E-07
          Group  19 Cat  2 92235    16 9.7202E-07
          Group  19 Cat  1 92238    16 9.7202E-07
          Group  20 Cat  2 92235    16 6.2978E-07
          Group  20 Cat  1 92238    16 6.2978E-07
          Group  21 Cat  2 92235    16 8.5688E-07
          Group  21 Cat  1 92238    16 8.5688E-07
          Group  22 Cat  2 92235    16 6.2978E-07
          Group  22 Cat  1 92238    16 6.2978E-07
          Group  23 Cat  2 92235    16 6.3418E-07
          Group  23 Cat  1 92238    16 6.3418E-07
          Group  24 Cat  2 92235    20 6.6917E-10
          Group  24 Cat  1 92238    20 6.6918E-10
          Group  25 Cat  2 92235    16 8.7118E-07
          Group  25 Cat  1 92238    16 8.7118E-07
          Group  26 Cat  2 92235    16 9.8351E-07
          Group  26 Cat  1 92238    16 9.8351E-07
          Group  27 Cat  2 92235    20 2.6513E-08
          Group  27 Cat  1 92238    20 2.6513E-08
          Group  28 Cat  2 92235    16 6.2978E-07
          Group  28 Cat  1 92238    16 6.2978E-07
          Group  29 Cat  2 92235    16 6.2978E-07
          Group  29 Cat  1 92238    16 6.2978E-07
          Group  30 Cat  2 92235    20 6.4310E-09
          Group  30 Cat  1 92238    20 6.4310E-09
          Group  31 Cat  2 92235    16 6.2978E-07
          Group  31 Cat  1 92238    16 6.2978E-07
          Group  32 Cat  2 92235    16 6.5474E-07
          Group  32 Cat  1 92238    16 6.5474E-07
          Group  33 Cat  2 92235    20 4.3886E-08
          Group  33 Cat  1 92238    20 4.3886E-08
          Group  34 Cat  2 92235    20 6.9230E-07
          Group  34 Cat  1 92238    20 6.9230E-07
          Group  35 Cat  2 92235    20 1.5370E-08
          Group  35 Cat  1 92238    20 1.5370E-08
          Group  36 Cat  2 92235    16 6.2978E-07
          Group  36 Cat  1 92238    16 6.2978E-07
          Group  37 Cat  2 92235    16 6.8387E-07
          Group  37 Cat  1 92238    16 6.8387E-07
          Group  38 Cat  2 92235    16 6.2978E-07
          Group  38 Cat  1 92238    16 6.2978E-07
          Group  39 Cat  2 92235    16 6.2978E-07
          Group  39 Cat  1 92238    16 6.2978E-07
          Group  40 Cat  2 92235    16 6.3269E-07
          Group  40 Cat  1 92238    16 6.3269E-07
010:34:51 Using P0 in All Regions...
010:34:51 @t= 6.00000E-01 p= 9.31895E+01   5
010:35:02 Finished
```